PTEN is recruited to the postsynaptic terminal for NMDA receptor-dependent long-term depression

Sandra Jurado[2,3], Marion Benoist[1], Argentina Lario[1], Shira Knafo[1], Cortney N. Petrok[2] and José A. Esteban[1*].

[1]Centro de Biología Molecular "Severo Ochoa", Consejo Superior de Investigaciones Científicas (CSIC), Universidad Autónoma de Madrid, Madrid 28049, Spain

[2]Department of Pharmacology, University of Michigan Medical School, Ann Arbor, MI 48109, USA

[3]Present address: Department of Psychiatry & Behavioral Science, Stanford School of Medicine, Palo Alto, California 94304, USA

Running title: PTEN is recruited to synapses for LTD

[*]Correspondence should be addressed to J.A.E. (jaesteban@cbm.uam.es), Centro de Biología Molecular "Severo Ochoa", Consejo Superior de Investigaciones Científicas (CSIC), Universidad Autónoma de Madrid, Madrid 28049, Spain.

Character count: 54,984

Subject categories: Neuroscience, Membranes & Transport

ABSTRACT

PTEN is a key regulator of PIP_3 signaling, which controls cell growth and differentiation. However, PTEN is also highly expressed in the adult brain, where it can be found in dendritic spines in hippocampus and other brain regions. Here, we have investigated specific roles of PTEN in the regulation of synaptic function in excitatory hippocampal synapses. We found that NMDA receptor activation triggers a PDZ-dependent association between PTEN and the synaptic scaffolding molecule PSD-95. This association is accompanied by PTEN localization at the postsynaptic density and anchoring within the spine. On the other hand, enhancement of PTEN lipid phosphatase activity is able to drive depression of AMPA receptor-mediated synaptic responses. This activity is specifically required for NMDA receptor-dependent LTD, but not for LTP or mGluR-dependent LTD. Therefore, these results reveal PTEN as a regulated signaling molecule at the synapse, which is recruited to the postsynaptic membrane upon NMDA receptor activation, and is required for the modulation of synaptic activity during plasticity.

Keywords: hippocampus/LTD/AMPA receptors/NMDA receptors/spines

INTRODUCTION

PTEN (Phosphatase and Tensin Homolog Deleted on Chromosome Ten; also known as MMAC1 or TEP1) was originally cloned as a tumor suppressor protein (Li et al., 1997; Steck et al., 1997). PTEN antagonizes phosphatidylinositosl-3'-kinase (PI3K) signaling by dephosphorylating phosphatidylinositol-(3,4,5,)-trisphosphate (PIP_3) to generate phosphatiylinositol-(4,5)-bisphosphate (PIP_2) (Maehama and Dixon, 1999). As a negative regulator of the PI3K-PIP_3 pathway, PTEN restrains cell proliferation and survival during embryogenesis. Consistent with this developmental role, PTEN *null* mice die during embryogenesis, while heterozygotes are tumor-prone and display enlargement of multiple organs (Stiles et al., 2004). Similarly, alterations in the function of PTEN are of major relevance for the incidence of a wide variety of human cancers (Li et al., 1997; Pendaries et al., 2003).

In the central nervous system, PTEN is expressed in most, if not all neurons. It is present in dendrites and spines of cerebral cortex, cerebellum, hippocampus and olfactory bulb (Perandones et al., 2004). Mutation or inactivation of PTEN contributes to brain tumors, macrocephaly, seizures and ataxia (Backman et al., 2001; Eng, 2003; Kwon et al., 2001). PTEN mutations have been also associated with mental retardation and autism spectrum disorders (Butler et al., 2005; Kwon et al., 2006). At the cellular level, neurons lacking PTEN develop larger and more branched dendrites, which harbor more synapses (Fraser et al., 2008; Jaworski et al., 2005; Kwon et al., 2006). Therefore, it is likely that the neurological deficits associated to PTEN mutations are derived from aberrant neuronal growth and connectivity during brain development. These widespread morphological changes may also be the reason for the pleiotropic effects on synaptic function and plasticity that have been reported for mice with reduced PTEN expression (Fraser et al., 2008; Wang et al., 2006).

Besides these developmental aspects, the PIP_3 pathway has specific functions at synapses in differentiated neurons. For example, acute blockade of PI3K, the PIP_3 synthesizing enzyme, has been shown to impair some forms of memory formation (Chen et al., 2005) and long-term potentiation (LTP) in hippocampal slices (Cammalleri et al., 2003; Opazo et al., 2003; Sanna et al., 2002; Tang et al., 2002). The PIP_3 pathway has also been linked to AMPAR trafficking (Qin et al., 2005) and synaptic localization (Arendt et al., 2010) in hippocampal neurons. However, a specific role for PTEN in synaptic transmission or plasticity in developed neurons has not been pinpointed yet.

From a mechanistic point of view, PTEN possesses a PDZ binding motif at its C-terminus (residues Thr^{401}-Lys^{402}-Val^{403}-COOH), which interacts with multiple PDZ domain-containing proteins, such as the scaffolding proteins MAGI-1/2/3, hDlg/SAP97 and the Ser/Thr kinase MAST205 (Bonifant et al., 2007). The physiological consequences of these PDZ-dependent interactions remain poorly characterized; however it has been shown that the binding of PTEN to specific PDZ domain-containing proteins contributes to PTEN protein stability (Valiente et al., 2005). Nevertheless, no interaction between PTEN and synaptic PDZ proteins has been reported yet.

In the present study, we have investigated specific roles of PTEN in synaptic plasticity, separate from its developmental functions. In particular, we have found that NMDA receptor activation triggers the association between PTEN and PSD-95 through a PDZ-dependent interaction. This interaction leads to the recruitment and anchoring of PTEN to the postsynaptic membrane, and possibly mediates a specific role of PTEN in the expression of LTD. These results have revealed PTEN as a regulated component of the intracellular signaling machinery that controls synaptic transmission and plasticity at hippocampal excitatory synapses.

RESULTS

NMDA receptor activation regulates a PDZ-dependent association between PTEN and PSD-95

As an initial step to evaluate potential functions of PTEN at synapses, we tested its association with PSD-95, a critical regulator of synaptic function and plasticity (Bhattacharyya et al., 2009; Ehrlich and Malinow, 2004; El-Husseini et al., 2000). To this end, we immunoprecipitated PTEN from total hippocampal extracts, and the presence of co-immunoprecipitated proteins was analyzed by western blot (see Methods). As shown in Fig. 1A (upper panels, "Control" lanes), there was a detectable association between PSD-95 and PTEN, which was specific, according to the immunoprecipitation with a non-immune ("n.i.") antibody. Interestingly, the association between PSD-95 and PTEN appeared to be regulated by activity, since it was increased after 5 min bath-application of 20 μM NMDA (Fig. 1A, compare "Control" and "NMDA" lanes), and this increase was abolished by incubation with the NMDAR antagonist AP5 (Fig. 1B, "NMDA+AP5" lanes). There was also a weak, but detectable, interaction between PTEN and MAGI-2, another PDZ protein known to associate with PTEN (Wu et al., 2000). However, this interaction was not altered by NMDAR activation (Fig. 1A, middle panels).

We then tested whether the association between PSD-95 and PTEN was specifically regulated by NMDAR activation or whether it could also be induced by other forms of neuronal activation or depolarization. To this end, we compared the amount of PTEN-PSD-95 co-immunoprecipitation from slices incubated for 5 min with NMDA (20 μM), AMPA (100 μM) or KCl (50 mM). A control immunoprecipitation with a non-immune antibody was also carried out. Interestingly, the association between PTEN and PSD-95 was only enhanced in slices treated

with NMDA, but not with AMPA or KCl (Fig. 1C, right panel; total protein inputs for all conditions are shown in the left panel). In order to evaluate the time course of this association, we carried out immunoprecipitations at different times after the 5 min incubation with NMDA. As shown in Fig. 1D, E, the association between PTEN and PSD-95 persists for a period of time after the end of NMDAR activation, although it gradually declines by the end of the time course. It should also be pointed out that the fraction of PSD-95 associated with PTEN is rather low at all times: around 1% of the total PSD-95 under basal conditions, roughly doubling after NMDA induction (see quantification in Fig. 1E). The regulated association between PSD-95 and PTEN was also observed after immunoprecipitation of PSD-95 and detection of PTEN as a co-precipitated protein (Supplementary Fig. 1). This regulation appears to be specific for PTEN, because the interaction of PSD-95 with another PDZ-dependent partner (the NMDA receptor) was not enhanced by this treatment (Supplementary Fig. 1, PTEN *versus* GluN1 panels).

To further characterize the structural requirements of this regulated association between PSD-95 and PTEN, we expressed GFP-tagged PTEN in organotypic slice cultures of rat hippocampus for 15 to 20 hours (GFP is fused to the N-terminus of PTEN). Confocal imaging of infected CA1 neurons showed widespread distribution of GFP-PTEN, including distal dendrites and spines (Fig. 1F). Recombinant GFP-PTEN was functional, as evidenced from its ability to antagonize the PI3K/PIP_3 pathway, leading to a decrease in Akt phosphorylation at Ser473 (Stambolic et al., 1998) (Supplementary Fig. 2A, B). Total protein extracts were prepared from untreated slices or from slices treated with NMDA, AMPA or KCl, as described above. Immunoprecipitations were carried out with an anti-GFP antibody, and the immunoprecipitated fractions were analyzed by western blot. As shown in Fig. 1G, PSD-95 was co-precipitated with GFP-PTEN only after NMDAR activation, but not after AMPA or KCl treatment, similar to the

results obtained with endogenous PTEN (Fig. 1C). The kinetics of GFP-PTEN association with PSD-95 were also similar to the endogenous protein (Fig. 1H, right panels; inputs for all conditions are shown in the left panels). As control, cytosolic GFP did not co-immunoprecipitate with PSD-95 with or without NMDA (Fig. 1H).

PDZ-dependent interactions anchor PTEN at dendritic spines upon NMDA receptor activation

To determine whether the association between PTEN and PSD-95 was PDZ-dependent, we generated a PTEN mutant lacking the last four amino acids, which contain the PDZ ligand motif (-ITKV*). We then carried out co-immunoprecipitations from slices expressing GFP, full-length GFP-PTEN or the truncated form of PTEN lacking its PDZ binding motif (GFP-PTEN-ΔPDZ) (see Supplementary Fig. 2C for a western blot analysis of the expression of this and other PTEN derivatives used in this study). As shown in Fig. 2A (upper right panel), the association with PSD-95 was only detectable with GFP-PTEN, but not with GFP-PTEN-ΔPDZ or cytosolic GFP, and only after NMDAR activation. This result confirms that the association between PTEN and PSD-95 requires the PDZ motif at the PTEN C-terminus.

PSD-95 is a well-known synaptic scaffolding molecule that organizes multiple signaling complexes at the synapse (Sheng, 2001). Therefore, our biochemical results described above suggest that PTEN may be recruited and anchored at synapses after NMDAR activation. To test this possibility, we evaluated real-time dynamics of PTEN in dendritic spines using fluorescence recovery after photobleaching (FRAP; see fluorescence images from a representative experiment in Fig. 2B). GFP-tagged PTEN was expressed in organotypic hippocampal slices, and the NMDA treatment was carried out as described above. Spines expressing GFP-PTEN were

photobleached and the extent of fluorescence recovery was measured before and after NMDAR activation ("+5", "+15" and "+25" minutes; for simplicity, the "+15-min" time point is only shown in the summary Fig. 2F). As shown in Fig. 2C (white circles), approximately 50% of the GFP-PTEN signal is recovered in the spine over a time course of 10-20 s, arguing that 50% of GFP-PTEN is stable in spines (over this period of time) under basal conditions. Intriguingly, GFP-PTEN fluorescence recovered to a significantly greater extent (around 70%) 5 min after the NMDA treatment (Fig. 2C, red circles). This result indicates an increase in PTEN mobility rapidly after NMDAR activation. In contrast, 20-30 min after the NMDA treatment, the recovery of fluorescence of GFP-PTEN in the spine was drastically reduced (around 20%; Fig. 2C, dark red circles; Fig. 2F), implying that a larger fraction of PTEN is retained in spines in a long-lasting manner after NMDAR activation.

To test the role of PDZ interactions in this behavior, we carried out similar experiments with the truncated form of PTEN lacking the PDZ motif, GFP-PTEN-ΔPDZ. As shown in Fig. 2D, the extent of fluorescence recovery was also greater 5 min after NMDAR activation (60% at baseline –white circles- *versus* 90% 5 min after the NMDA treatment –red circles-). But in marked contrast with full-length PTEN, this increase in PTEN mobility was long lasting (20-30 min after the NMDA treatment) and was never followed by an enhanced retention in spines (Fig. 2D, dark red circles; Fig. 2F).

As a control for potential changes in fluorophore diffusion in spines as a result of NMDA application, we carried out similar NMDA-FRAP experiments in slices expressing GFP. As shown in Fig. 2E, F, fluorescence recovery was nearly complete for GFP and was not altered at any time point in response to the NMDA treatment. In addition, neither the rates of recovery nor

the net distribution between spines and dendrites were significantly altered for any of the recombinant proteins after the NMDA treatment (Supplementary Fig. 3A and B, respectively).

Therefore, we conclude that NMDAR activation triggers a biphasic regulation of PTEN mobility in dendritic spines. First, there is a rapid and transient increase in mobility, which is independent from PDZ interactions. This phase is then followed by a longer-lasting and PDZ-dependent anchoring of PTEN at the spine (Fig. 2F).

Biochemical association of PTEN with the postsynaptic density (PSD) after NMDA receptor activation

To further investigate the recruitment of PTEN to the postsynaptic machinery upon NMDAR activation, we evaluated its association with the PSD using standard fractionation methods (Carlin et al., 1980). To this end, we isolated synaptosomal fractions from 3-4 weeks rats (see Supplementary Methods). NMDARs were then activated on the purified synaptosomes by adding 20 μM NMDA and 10 μM glycine. After 5 min incubation, NMDAR activation was stopped with AP-5 and synaptosomes were incubated for 10 more minutes to allow for PTEN stabilization. Then, the PSD fraction was isolated as a Triton-insoluble pellet from treated and untreated synaptosomes, and was analyzed by western blot (see Supplementary Methods).

As shown in Fig. 3, the abundance of PTEN at the PSD was significantly enhanced (2-fold) on the synaptosomes treated with NMDA plus glycine. The PSD enrichment of other postsynaptic markers was not altered (PSD-95) or was slightly decreased (GluN1 and αCaMKII) with this treatment, ruling out potential artifacts due to non-specific protein aggregation or precipitation. In conclusion, these experiments indicate that PTEN biochemically associates with

the PSD scaffold after NMDAR activation, in agreement with its co-precipitation with the PSD-95 protein complex.

Local redistribution of PTEN within dendritic spines in response to NMDAR activation

In order to directly visualize the recruitment of PTEN to the postsynaptic scaffold, we evaluated the ultrastructural localization of endogenous PTEN within dendritic spines before and after NMDA treatment. PTEN has been described to be present in axonal and dendritic compartments in hippocampal neurons (Perandones et al., 2004), but the fine-scale distribution of PTEN in dendritic spines had never been evaluated before.

We characterized the ultrastructural distribution of endogenous PTEN in close proximity to synaptic sites using postembedding immunogold electron microscopy (see Methods, and Fig. 4A for representative micrographs). Most synaptic PTEN immunolabeling was found in the postsynaptic terminal (70% *versus* 30% presynaptic; Fig. 4B). Within the postsynaptic compartment, PTEN labeling was predominantly located in the intracellular space of the spine (Fig. 4B, "Intra"), outside of the postsynaptic density (PSD) and the extrasynaptic membrane ("Extra").

Remarkably, upon NMDAR activation (25 min after the NMDA treatment), PTEN fraction in the PSD increased by 6-fold, while the amount of PTEN in other synaptic compartments was not significantly affected (Fig. 4B, black columns; representative micrographs in Fig. 4A). In addition, and consistent with this redistribution of PTEN into the PSD, we observed a global shift in the population of PTEN molecules towards the PSD (Fig. 4C).

Therefore, and in agreement with our biochemical and fluorescence imaging data, these data confirm that endogenous PTEN redistributes to the postsynaptic membrane in response to NMDAR activation.

Enhancement of PTEN activity depresses AMPA receptor-mediated synaptic transmission

As an initial step to examine PTEN function in synaptic transmission, we overexpressed wild-type GFP-PTEN or a catalytically dead mutant (GFP-PTEN-C124S) in CA1 neurons from organotypic slice cultures. Importantly, expression of this mutant produced an increase in phospho-Akt over basal levels (Supplementary Fig. 2A, B), indicating that this construct behaves as a dominant negative against endogenous PTEN activity in neurons, as it has been described previously in other cell types (Maehama and Dixon, 1998).

The effect of GFP-PTEN and GFP-PTEN-C124S on synaptic transmission was evaluated by simultaneous double whole-cell recordings from pairs of nearby infected and uninfected CA1 neurons, under voltage clamp configuration, while stimulating presynaptic Schaffer collateral fibers (to note, under this configuration, the recombinant proteins are always expressed exclusively in the postsynaptic neuron). As shown in Fig. 5A-C, PTEN overexpression produced a significant depression of AMPAR-mediated currents as compared to uninfected cells, whereas NMDAR responses remained unchanged. In contrast, the catalytically dead mutant, PTEN-C124S, did not alter AMPAR- or NMDAR-mediated transmission (Fig. 5D-F). This result verifies that the catalytic activity of PTEN is required for the depression of AMPAR-mediated transmission, and that this is not due to virus infection or nonspecific sequestration of regulatory proteins. Importantly, passive membrane properties, such as input resistance and holding current

(related to basal ionic conductances), and whole-cell capacitance (related to cell size) were also similar in control and in PTEN–overexpressing neurons (Supplementary Fig. 4).

Intriguingly, the depression of AMPAR responses produced by overexpression of PTEN was observed for basal synaptic transmission, that is, conditions under which PTEN is not normally recruited to the postsynaptic membrane (previous biochemical and imaging experiments). One possible explanation is that overexpressed PTEN is able to reach the postsynaptic membrane in the absence of its regulated association with PDZ proteins at the postsynaptic scaffold. To test this possibility, we carried out similar recordings with neurons overexpressing the truncated PTEN mutant lacking the PDZ motif (PTEN-ΔPDZ). As shown in Fig. 5G-I, overexpressed PTEN was able to depress AMPAR responses in the absence of PDZ-dependent interactions. This depression was still specific for AMPARs, as compared to NMDARs. Therefore, although the recruitment of PTEN to the synaptic scaffold requires NMDAR activation and PDZ-dependent interactions, these requirements can be overcome by overexpression of the recombinant protein.

The depression of basal synaptic responses produced by PTEN might be a consequence of an abnormal cycling of AMPARs at synapses. AMPARs are believed to cycle continuously in and out of synapses in an activity-independent manner, which depends on the interaction between the GluA2 subunit (also known as GluR2 (Collingridge et al., 2009)) and NSF (N-ethylmaleimide-sensitive fusion protein) (Luscher et al., 1999; Nishimune et al., 1998; Song et al., 1998). When this interaction is impaired by intracellular infusion of a peptide containing the NSF-binding sequence of GluA2 (pep2m/G10), AMPAR-mediated synaptic transmission rapidly “runs down” as the receptors continue to be internalized but fail to be reinserted at the synaptic membrane (Luscher et al., 1999; Nishimune et al., 1998). We have used the same approach to

determine whether PTEN affects the constitutive cycling of AMPA receptors. To this end, we recorded AMPAR-mediated synaptic responses from CA1 hippocampal neurons infected with PTEN while infusing them with the GluA2-NSF peptide pep2m/G10. The peptide produced a fast "run-down" of synaptic transmission in the uninfected cells (Fig. 5J, white symbols), as expected. This "run-down" was virtually identical in the cells expressing PTEN (Fig. 5J, black symbols), indicating that PTEN activity does not alter the continuous cycling of AMPARs.

Although PTEN was expressed in postsynaptic CA1 neurons, we examined whether presynaptic properties may have been altered retrogradely (Futai et al., 2007; Regalado et al., 2006). As shown in Fig. 5K, paired pulse facilitation (PPF), an indicator of presynaptic function, was unaltered by PTEN overexpression.

The PIP_3 pathway is also involved in the regulation of gene expression (Brunet et al., 2001). Nevertheless, overnight overexpression of PTEN did not affect the expression levels of GluA1 and GluA2 subunits of AMPA receptors, or their phosphorylation state (phospho-Ser 831 and 845 for GluA1, and phospho-Ser 880 for GluA2; Supplementary Fig. 5).

Therefore, these combined data strongly suggest that PTEN plays a specific postsynaptic role at excitatory hippocampal synapses.

PTEN activity is required for NMDA receptor-dependent LTD

The depression of AMPAR responses as a consequence of PTEN overexpression led us to think that this phosphatase may play a role in long lasting changes of synaptic strength, and particularly, in long-term depression (LTD). In addition, the NMDA treatments that we found to regulate the association of PTEN with postsynaptic elements (Figs. 1 and 3) and its redistribution in spines (Figs. 2 and 4) are known to lead to synaptic depression (Lee et al., 1998).

To directly test a potential role of PTEN in LTD in hippocampal slices, we used a bis-peroxivanadium derivative, bpV(HO)pic, which has been shown to specifically inhibit PTEN when used at a low nanomolar concentrations (Schmid et al., 2004) (see Supplementary Fig. 6 for a test of bpV(HO)pic specificity). LTD was induced on control or on bpV(HO)pic-pretreated slices by pairing presynaptic stimulation (1 Hz, 500 pulses) with moderate postsynaptic depolarization (-40 mV). Interestingly, when compared to control cells, inhibition of PTEN with bpV(HO)pic greatly reduced the magnitude of LTD (Fig. 6A, D), suggesting that PTEN activity is necessary for LTD in CA1 hippocampal synapses (bpv(HO)pic did not have significant effect on the control pathway –Fig. 6D- or on basal synaptic transmission –not shown). Similar blockade of LTD expression was observed when the PTEN inhibitor was applied only during the time of LTD induction (see Supplementary Fig. 7).

As an alternative approach to test the role of PTEN in LTD, we carried out similar experiments with neurons expressing the catalytically dead mutant PTEN-C124S. It is important to keep in mind that this mutant did not have any effect on basal AMPAR- or NMDAR-mediated transmission (Fig. 5D-F). Interestingly, PTEN-C124S displayed a dominant negative effect on LTD. That is, PTEN-C124S expression blocked LTD to a similar extent as the PTEN inhibitor (Fig. 6B, D).

PTEN is known to have both lipid and protein phosphatase activity, as well as phosphatase-independent functions (Tamguney and Stokoe, 2007). To test whether the role of PTEN in LTD was specifically dependent on its PIP_3-phosphatase activity, we used a lipid phosphatase PTEN mutant that retains its protein phosphatase activity: PTEN-G129E (Myers et al., 1998). Similar to our results with PTEN-C124S, neurons expressing PTEN-G129E did not undergo long lasting depression (Fig. 6C, D). Taken together, these pharmacological and genetic

approaches indicate that PTEN lipid phosphatase activity is required for LTD in CA1 hippocampal synapses.

To further explore the role of PTEN in synaptic depression, we evaluated LTD in neurons overexpressing wild-type PTEN. As shown in Supplementary Fig. 8, PTEN overexpression did not alter LTD expression. Taking into account that PTEN-overexpressing neurons display reduced AMPAR-mediated synaptic transmission under basal conditions (Fig. 5A, B), these data suggest either that PTEN-induced depression does not saturate subsequent LTD expression, or alternatively, that overexpressed PTEN acts on a different pool of AMPARs from those removed during synaptically induced LTD.

PTEN is neither required for LTP nor for mGluR-dependent LTD

After having established the importance of PTEN for LTD, we wished to investigate whether PTEN activity is required for LTP, another paradigmatic form of NMDAR-dependent synaptic plasticity. To this end, we evaluated the effect of the catalytically dead mutant, PTEN-C124S, on LTP in CA1 hippocampal neurons. LTP was induced on infected and uninfected CA1 neurons by pairing presynaptic stimulation (3 Hz, 300 pulses) with postsynaptic depolarization (0 mV). As shown in Fig. 7A, C, no significant difference was found between uninfected (control) and infected (PTEN-C124S-expressing) neurons. PTEN-C124S did not have any effect on the non-potentiated (unpaired) pathway either (Fig. 7C). Virtually identical results were obtained with the specific PTEN inhibitor bpV(HO)pic (Fig. 7B, C). Therefore, these data indicate that PTEN is required specifically for LTD, and not for other forms of NMDAR-dependent synaptic plasticity.

In addition, we tested whether PTEN would be required for another prominent form of LTD in CA1 hippocampal synapses, which is dependent on the activation of metabotropic glutamate receptors (mGluRs) (Oliet et al., 1997; Palmer et al., 1997). mGluR-dependent LTD was induced by bath application of 50 μM DHPG (group I mGluR agonist) in the presence of 100 μM AP5 (NMDAR antagonist) (see Methods). As shown in Fig. 7D, F, neurons expressing the catalytically dead PTEN-C124S displayed similar depression to the control, uninfected neurons. Again, identical results were obtained when blocking PTEN activity pharmacologically (Fig. 7E, F). Therefore, we conclude that PTEN is not required for mGluR-dependent LTD in CA1 neurons.

Involvement of PDZ-dependent interactions of PTEN during NMDAR-dependent LTD

Our electrophysiological data shown above indicate that PTEN activity is specifically required for NMDAR-dependent LTD, but not for basal synaptic transmission or for other forms of synaptic plasticity. In part, these conclusions are based on the observation that catalytically inactive forms of PTEN have a dominant negative effect on endogenous PTEN to block NMDAR-dependent LTD (Fig. 6B, C). In other words, these PTEN mutants appear to be competing with endogenous PTEN for some important interaction required for LTD. An obvious candidate for this interaction is the PDZ motif at the C-terminus of PTEN, which we have found mediates the anchoring of PTEN in the spine and its association with PSD-95 upon NMDAR activation (Fig. 2).

In order to investigate whether PDZ-dependent interactions of PTEN are important for its role in LTD, we tested whether the dominant negative effect of PTEN-C124S requires its PDZ C-terminal motif. To this end, we generated a catalytically dead mutant (C124S) lacking the PDZ

ligand motif (-ITKV*). This mutant (PTEN-C124S-ΔPDZ) did not affect basal synaptic transmission mediate by AMPA or NMDA receptors (Fig. 8A-C), consistent with the results with PTEN-C124S (Fig. 5D-F). Then, we carried out LTD experiments in CA1 neurons expressing this truncated, catalytically dead mutant. Interestingly, neurons expressing PTEN-C124S-ΔPDZ displayed normal LTD, undistinguishable from uninfected cells (Fig. 8D, E). Therefore, these results suggest that the C-terminal PDZ binding motif of PTEN is necessary for its function in LTD.

DISCUSSION

In this study we show that the lipid phosphatase PTEN, typically associated with cell growth and proliferation, is recruited to synapses and is required for the expression of NMDAR-dependent LTD. This is based on three main lines of evidence. First, using electrophysiological assays on hippocampal slices, we have determined that enhancement of PTEN activity is sufficient to depress AMPAR-mediated synaptic transmission, and that PTEN lipid phosphatase activity is specifically required for NMDAR-dependent LTD. Second, a combination of live imaging, electron microscopy and biochemical assays indicate that NMDAR activation triggers a PDZ-dependent association between PTEN and the synaptic scaffold, which anchors PTEN at the postsynaptic terminal. And third, this PDZ-dependent interaction appears to be involved in PTEN's action during LTD, since a dominant negative mutant of PTEN is ineffective when lacking its PDZ motif. These combined results reveal PTEN as a regulated signaling molecule at synapses, which is recruited to the postsynaptic membrane in an activity-dependent manner and is required for the modulation of synaptic activity during plasticity.

An important aspect of this work is the identification of a precise synaptic function for PTEN during plasticity. PTEN is a well-known negative regulator of PI3K signaling, and as such, it controls multiple aspects of neuronal development, including neurite growth, axon specification, dendritic arborization and growth cone dynamics (Chadborn et al., 2006; Jaworski et al., 2005; Kwon et al., 2006). In this context, it may not be surprising that previous studies using heterozygous or mosaic PTEN knock-out mice have reported multiple impairments in synaptic function, including basal transmission, paired-pulse facilitation, LTP and LTD (Fraser et al., 2008; Wang et al., 2006). These complex phenotypes are probably related to general neuronal dysfunctions caused by alterations in the PIP_3 pathway during development. Our data presented here indicate that semi-acute (15 to 20 hours) blockade of PTEN activity, either through pharmacological or genetic approaches, results in a very specific impairment of NMDAR-dependent LTD, without affecting basal synaptic transmission, NMDAR function, LTP, mGluR-dependent LTD or presynaptic function. Therefore, we believe that these results are revealing an acute and distinct role of PTEN at otherwise unperturbed synapses.

Perhaps one of the most surprising observations of this study is the recruitment of PTEN to the postsynaptic complex in response to NMDAR activation. PTEN was already known to interact with PDZ domain-containing proteins in different cell types (Bonifant et al., 2007). However, no such interaction had been reported in neurons before this work. We now identify PSD-95 as a potential PDZ synaptic partner for PTEN. This association is very low under basal conditions, but it is rapidly triggered upon NMDAR activation. We should also point out that our results do not prove a direct interaction between PTEN and PSD-95. Given the dense network of interactions present at the postsynaptic membrane, it is possible that the association between PTEN and PSD-95 is just reflecting the recruitment of PTEN to the postsynaptic scaffold.

Indeed, this recruitment may be maintained by different sets of interactions at different time points, since the anchoring of PTEN in spines and its presence at the postsynaptic density (fluorescence and electron microscopy data) appears to be longer lasting than its association with PSD-95 (co-immunoprecipitations). This interpretation would also fit with previous reports showing that PSD-95 is partially removed from spines during LTD (Bhattacharyya et al., 2009; Horne and Dell'Acqua, 2007; Sturgill et al., 2009).

The regulation of PTEN interactions during LTD is likely to occur at multiple levels. For example, we have observed that NMDAR activation triggers a transient mobilization of PTEN within dendritic spines, which precedes its PDZ-dependent anchoring. Therefore, it is likely that the regulation of PTEN in response to NMDAR activation will involve release from basal retention interactions, as well as association with new synaptic partners. In fact, the initial mobilization of PTEN may facilitate its subsequent association with PSD-95 at the PSD. Undoubtedly, further work will be required to dissect the details of this dynamic behavior of PTEN within dendritic spines. Nevertheless, these new results strengthen the emerging notion that PSD-95 acts as an important organizer of synaptic signaling during LTD (Bhattacharyya et al., 2009; Xu et al., 2008).

What are the functional consequences of this activity-dependent recruitment of PTEN to the postsynaptic complex? It is reasonable to hypothesize that binding of PTEN to the postsynaptic complex positions PTEN in close proximity to the postsynaptic membrane, which in turn would facilitate access to its PIP_3 substrate during NMDAR-dependent LTD. On the one hand, the stabilization of PTEN in close proximity to its substrate could have significant effects on its catalytic efficiency. But perhaps more importantly, this mechanism would also restrict PTEN action to the postsynaptic membrane of the synapses being activated. In other words, this

regulated PDZ-dependent recruitment of PTEN may provide the means to achieve synapse-specific modulation of PIP_3 signaling during plasticity.

And finally, how does PTEN activity lead to LTD expression? We have recently described that downregulation of PIP_3 leads to the redistribution of AMPARs from the postsynaptic membrane into the extrasynaptic surface of the spine (Arendt et al., 2010). On the one hand, this short-range movement is expected to depress synaptic transmission, as perisynaptic AMPARs will not be significantly activated by synaptically released glutamate (Raghavachari and Lisman, 2004). On the other hand, this redistribution of AMPARs may facilitate their access to perisynaptic endocytic hotspots (Blanpied et al., 2002; Petralia et al., 2003; Racz et al., 2004), and therefore may act as an initial step preceding AMPAR internalization.

A downstream effector of the PIP_3 pathway is glycogen synthase kinase-3 β (GSK-3β). Upregulation of PIP_3 levels leads to activation of the Ser/Thr kinase Akt, which in turns phosphorylates and inactivates GSK-3β (Cross et al., 1995). Therefore, PTEN will act as a positive regulator of GSK-3β, by reducing PIP_3 levels with the concomitant decrease in Akt activation and dephosphorylation (activation) of GSK-3β. Interestingly, GSK-3β has been recently shown to be activated (dephosphorylated) upon LTD induction and this activation was required for the specific expression of LTD (*versus* LTP) (Peineau et al., 2007). Therefore, it is possible that the recruitment of PTEN to the postsynaptic membrane during LTD is relayed through the PIP_3 pathway to activate GSK-3β at specific synapses. This mechanism would be consistent with the presence of GSK-3β in synaptosomal preparations and dendritic spines (Hooper et al., 2007; Peineau et al., 2007). Therefore, our results propose a specific mechanism for the synaptic compartmentalization of PIP_3 signaling during plasticity.

In addition, it has been recently shown that LTD requires PIP_2 turnover by phospholipase C (PLC), which leads to the loss of the scaffolding molecules AKAP79 and PSD-95 from synapses and initiates the structural remodeling of the spine (Horne and Dell'Acqua, 2007). Taking together, Dell'Acqua's study and ours would suggest an interesting relay of phosphoinositide metabolism during LTD, which would involve degradation of PIP_3 into PIP_2 (*via* PTEN) for initial AMPAR depression, and subsequent PIP_2 turnover (*via* PLC) for further structural and functional changes in the spine.

In summary, this work has offered new insights into the organization of synaptic signaling during plasticity, and has revealed distinct roles for the tumor suppressor PTEN as a critical mediator of long-term depression in hippocampal neurons.

MATERIALS AND METHODS

Expression of recombinant proteins and antibodies used in this study are described in Supplementary Methods.

Co-immunoprecipitations and pharmacological treatments

Hippocampal slices were transferred to a submersion-type holding chamber containing artificial cerebrospinal fluid (ACSF, composition described in Supplementary Information), gassed with 5% CO_2 / 95% O_2 at 30°C. Slices were equilibrated in the holding chamber for 10 minutes prior to each experiment and were transferred to a separate chamber containing ACSF plus 20 μM NMDA, 100 μM AMPA or 50 mM KCl, where they remained for 5 minutes. Following these treatments, some slices were taken immediately for homogenization in a buffer containing: 10 mM HEPES, 150 mM NaCl, 10 mM EDTA, 0.1 mM phenylmethanesulphonylfluoride (PMSF), 2 μg/ml of chymostatin, leupeptin, antipain and pepstatin, 10 mM NaF, 1 μM microcystin LR, 0.5 μM calyculin A and 1 % Triton X-100. Other slices were transferred to another chamber containing ACSF, for variable recovery times, as indicated in each experiment. Total protein extracts were prepared in the buffer described above. For immunoprecipitations, 200-300 μg of protein extracts were incubated with the corresponding antibodies and with 40 μl of protein G-sepharose beads (50%) (Amersham Biosciences), for 4 hours at 4°C. These samples were then washed and immunoprecipitated proteins were eluted by boiling in 1x Laemmli sample buffer and separated by SDS-PAGE. Visualization of immunoprecipitated proteins was done by western blot developed with chemiluminescence or with the Odyssey fluorescence system, and quantified with Image J under linear conditions.

Electrophysiology

Voltage-clamp whole cell recordings were obtained from nearby infected and uninfected CA1 pyramidal neurons, under visual guidance using fluorescence and transmitted light illumination. Composition of ACSF and internal solution, and description of synaptic plasticity protocols are included in Supplementary Methods. Bipolar stimulating electrodes were placed over Schaffer collateral fibers between 250 and 300 μm from the CA1 recorded cells, and synaptic responses were evoked with single voltage pulses (200 μs, up to 30 V). Responses were collected at -60 mV and +40 mV and averaged over 50-100 trials. All electrophysiological data were collected with pCLAMP software (Molecular Devices).

Fluorescent Recovery After Photobleaching (FRAP)

Hippocampal slices (5-7 DIV) were perfused with ACSF for 15-30 minutes. Confocal images of dendritic spines were obtained on an Olympus FV500 confocal microscope using a 60x oil immersion objective. Digital images were acquired using the FluoView software. Following acquisition of baseline images, dendritic spines where photobleached for 5 seconds (approximate time to completely bleach fluorescence signal in the spine). Recovery of fluorescence in the spine was measured from images acquired up to 50 seconds after the photobleaching. After collecting several images from dendritic spines under baseline conditions, the perfusion solution was switched to an ACSF containing 20 μM NMDA. After 5 minutes of NMDA treatment, the slices were washed again with standard ACSF. Further FRAP images were acquired after 10, 20 and 30 minutes of the NMDA treatment. Images were reconstructed and analyzed using NIH Image J software.

Electron Microscopy

Rat hippocampus was fixed, dehydrated, and processed for postembedding immunogold labeling as previously described (Phend et al., 1995). Immunostaining was with anti-PTEN antibody (Neomarkers) followed by an anti-mouse secondary antibody coupled to 10 nm gold particles (Electron Microscopy Sciences). Images were acquired with a Philips CM-100 transmission electron microscope coupled to a Kodak 1.6 Megaplus digital camera. Quantification of gold particles and distance measurements were carried out on the digital images using NIH Image J software.

Statistical analysis

Statistical differences were calculated according to non-parametric tests. Comparisons between multiple groups were carried out with the Kruskal-Wallis ANOVA. When significant differences were observed, *p* values for pairwise comparisons were calculated according to two-tailed Mann-Whitney tests (for unpaired data) or Wilcoxon tests (for paired data). Comparisons between cumulative distributions (Fig. 4C) were calculated with the Kolmogorov-Smirnov test.

ACKNOWLEDGMENTS

We thank Kristin Arendt and members of the Esteban lab for their critical reading of this manuscript. We also thank M. D. Ledesma for her advice with the synaptosomal preparations. The monoclonal antibody against PSD-95 was developed by and obtained from the UC Davis/NIH NeuroMab Facility, supported by NIH grant U24NS050606 and maintained by the Department of Neurobiology, Physiology and Behavior, College of Biological Sciences, University of California, Davis, CA 95616. This work was supported by grants from the National Institute of Mental Health (MH070417) and the Spanish Ministry of Science and Innovation (SAF-2008-04616, SAF-2009-05558-E) to J.A.E. M.B., S.K. and A.L. are supported by the Spanish Ministry of Science and Innovation. M.B. is also the recipient of an award from the Fondation Bettencourt-Schuller (France).

Conflict of Interests: The authors declare that they have no conflict of interest.

FIGURE LEGENDS

Figure 1. NMDA receptor-dependent association between PTEN and PSD-95. A. Total protein extracts from hippocampal slices were immunoprecipitated with anti-PTEN or with a non-immune ("n.i") antibody ("Control" lanes). Some slices were treated with 20 μM NMDA for 5 min before the immunoprecipitation ("NMDA" lanes). For all western blots, immunoprecipitated proteins are shown in the right panels, and 10% of the inputs in the left panels. **B.** Similar to A, but some slices were preincubated with the NMDAR antagonist AP5 before and during the NMDA treatment ("NMDA+AP5"). **C.** Similar to A, with slices pre-treated for 5 min with 20 μM NMDA, 100 μM AMPA, 50 mM KCl, or left untreated ("Control"), as indicated. **D.** Similar to A, with untreated slices ("Control"), treated with 20 μM NMDA for 5 min ("NMDA"), or transferred to regular ACSF for 10 min (+10') or 25 min (+25') after the NMDA treatment. Star (*) indicates the position of the IgG used for immunoprecipitation. **E.** Quantification of the fraction of PSD-95 co-precipitated with PTEN (as percentage from the total PSD-95 amount in the input), from 5 independent experiments as the one shown in D. The 5 min NMDA treatment is represented with a black bar. **F.** Representative confocal image showing the distribution of recombinant GFP-PTEN in soma, dendrites and spines in a hippocampal neuron from organotypic slice cultures. **G.** Hippocampal slices expressing GFP-PTEN were treated for 5 min with 20 μM NMDA, 100 μM AMPA, 50 mM KCl or left untreated ("Control"), as indicated. Total protein extracts were immunoprecipitated with anti-GFP and analyzed by western blot with anti-PSD95 (upper panels) or anti-GFP antibodies (lower panels). Star (*) indicates the position of the IgG used for immunoprecipitation. **H.** Hippocampal slices expressing GFP or GFP-PTEN, as indicated, were left untreated ("Ctrl."), or

were treated with 20 μM NMDA for 5 min (”NMDA”), or were transferred to regular ACSF for 10 min after the NMDA treatment (+10’). Total protein extracts were immunoprecipitated with anti-GFP and analyzed as in D. Star (*) indicates the position of the IgG used for immunoprecipitation.

Figure 2. PDZ-dependent interactions and anchoring of PTEN in spines. A. Coimmunoprecipitation experiments were similar to those in Fig. 1H, with slices expressing GFP, GFP-PTEN or the PDZ truncated mutant GFP-PTEN-ΔPDZ. Slices were treated with 20 μM NMDA for 5 min (“+NMDA”) or left untreated (“Control”). Western blot is representative of 3 independent experiments. **B.** Representative confocal images from a FRAP experiment. Left panel (“baseline”) shows GFP-PTEN expression in a dendritic branch and its spines. A specific spine (white dashed circle) was bleached (“bleaching”) and its fluorescence partially recovered 40 s later (“recovery”). **C.** Quantitative analysis of FRAP experiments as the one shown in A. “Baseline” (white symbols) represents FRAP experiments on GFP-PTEN-expressing slices perfused with ACSF (untreated). The perfusion solution was then switched to ACSF containing 20 μM NMDA. 5 minutes later, the slices were washed again with standard ACSF. Further FRAP images were acquired after 5, 15 and 25 minutes of ACSF wash (“+5 min”, red symbols; “+25 min”, dark red symbols; the “+15 min” time courses are similar to the “+25 min” ones, and are only represented in the summary plot in F, for simplicity). GFP fluorescence in the spine was normalized to the fluorescence in the unbleached dendritic shaft to correct for ongoing bleaching during imaging. Average values ± s.e.m. are plotted normalized to the baseline before bleaching. Number of spines analyzed were 12 (“baseline”), 8 (“+5 min”) and 9 (“+25 min”) (different spines are imaged at each time point). **D, E.** Similar to C, with slices expressing GFP-PTEN-

ΔPDZ (D) or plain GFP (E). Number of spines analyzed for GFP-PTEN-ΔPDZ were 7 at each time point, and for GFP 6 ("baseline"), 5 ("+5 min") and 5 ("+25 min"). **F.** Recovery fractions from experiments shown in C-E were calculated from the fraction of fluorescence recovered 40 s (GFP-PTEN and GFP-PTEN-ΔPDZ) or 4 s (GFP) after photobleaching. These values are plotted for untreated slices (0 min) or at different times after the 5 min NMDA treatment (the "+15 min" is not plotted in panels C-E for simplicity). Average values ± s.e.m. are plotted for GFP-PTEN (black symbols), GFP-PTEN-ΔPDZ (grey symbols) and GFP (white symbols). Statistical significance was calculated with respect to the recovery fractions before NMDA treatment. There was no significant difference in the case of GFP-expressing neurons.

Figure 3. Enrichment of PTEN at the postsynaptic density fraction after NMDA receptor activation. A. Representative western blot analysis of PSD fractionations from synaptosomal preparations after NMDA receptor activation ("+NMDA") or untreated controls ("−NMDA"). A duplicate of separately treated or untreated samples is presented. The starting material (synaptosomal fraction) is shown in the left lane. **B.** Quantification of PSD enrichment in NMDA treated samples normalized to the untreated controls, from experiments as the one shown in A. "n" represents number of independent experiments. Statistical significance was determined according to the Wilcoxon test for pairs of treated-untreated samples.

Figure 4. Local redistribution of PTEN to the postsynaptic density after NMDA receptor activation. A. Representative micrographs of CA1 stratum radiatum excitatory synapses after postembedding labeling with anti-PTEN immunogold (arrows). Presynaptic terminal is marked with an asterisk (*). Note accumulation of PTEN labeling at the PSD after 5 min NMDA

treatment and 25 min recovery in ACSF ("+25 min"), with respect to untreated slices ("Baseline"). **B.** Quantification of PTEN immunogold labeling at different compartments from electron micrographs as the ones shown in A. "PRE": presynaptic terminal; "POST": postsynaptic terminal; "PSD": postsynaptic density; "Extra": perisynaptic membrane lateral from the PSD; "Intra": intracellular space within the spine. Percentage of immunogold labeling per synapse was calculated as the number of gold particles at each compartment divided by the total number of gold particles in each synaptic terminal (only gold particles within 1 μm of the synaptic membrane were used for this analysis). Average values ± s.e.m. are plotted for untreated slices ("Baseline", white columns) or for slices treated for 5 min with NMDA and recovered for 25 min in ACSF ("+25 min", black columns). "n" represents number of synaptic terminals. Statistical significance was calculated according to the Mann-Whitney test. **C.** Quantification of PTEN distribution within the spine. The distance to the synaptic cleft was calculated for each immunogold particle before ("Baseline", black line) or after NMDA treatment ("+25 min", grey line), and plotted as cumulative distributions. The average thickness of the PSD from our micrographs (37 nm) is indicated in the plot as a vertical grey bar. "n" represents number of gold particles. Statistical significance was calculated according to the Kolmogorov-Smirnov test.

Figure 5. Effects of GFP-PTEN expression on synaptic transmission. A. Sample traces of evoked AMPAR- and NMDAR-mediated synaptic responses recorded at -60 mV or +40 mV, respectively, from CA1 neurons expressing GFP-PTEN and neighboring control (uninfected) neurons. **B.** Average AMPAR-mediated current amplitude (peak of the synaptic response recorded at -60 mV) from pairs of uninfected and GFP-PTEN-expressing neurons. For B, C, E, F, H and I, "n" represents number of pairs of cells, and statistical significance was determined

with the Wilcoxon test for paired data. **C.** Average NMDAR-mediated current amplitude (recorded at +40 mV and measured at a latency of 60 ms) from pairs of uninfected and GFP-PTEN-expressing neurons. **D-F.** Similar to A-C, with infected neurons expressing GFP-PTEN-C124S. **G-I.** Similar to A-C, with infected neurons expressing GFP-PTEN-ΔPDZ. **J.** Time course of AMPAR-mediated synaptic responses recorded from CA1 neurons expressing GFP-PTEN or from control (uninfected) neurons, during whole-cell pipette infusion of the GluA2-NSF interfering peptide (pep2m). Response amplitude is normalized to a 2 min baseline from the beginning of the recording. "n" represents number of cells. Inset: sample traces averaged from the first 5 min of the recording (thin lines) or from the last 5 min of the time course (thick lines). **K.** Paired-pulse facilitation (PPF) recorded from control (uninfected) neurons or from neurons expressing GFP-PTEN. PPF is calculated as the ratio of the amplitude of the second response versus that of the first one. "n" represents number of cells. Inset: representative traces of evoked AMAR-mediated responses with an interstimulus interval of 200 ms.

Figure 6. PTEN lipid phosphatase activity is required for LTD. A-C. LTD was induced in CA1 hippocampal neurons pre-treated with the PTEN inhibitor bpV(HO)pic (A) or expressing the PTEN point mutants C124S (B) or G129E (C). Results from control neurons (uninfected or untreated) were carried out in an interleaved manner with their corresponding infected or treated neurons. Amplitude of the synaptic responses is normalized to a 10 min baseline. Insets: sample traces averaged from the baseline (thin lines) or from the last 10 min of the recording (thick lines). **D.** Average of AMPAR-mediated responses collected from the last 10 min of the recording and normalized to the baseline. Left columns (LTD, paired) correspond to the stimulation pathway in which postsynaptic depolarization (-40 mV) was paired to low-frequency

stimulation (1 Hz). Right columns (control, unpaired) correspond to the pathway that was not stimulated during depolarization. “n” represents number of cells.

Figure 7. PTEN activity is not required for LTP or for mGluR-dependent LTD. A. LTP was induced in CA1 hippocampal neurons expressing GFP-PTEN-C124S (black symbols) or in control (uninfected) neurons (white symbols). Amplitude of the synaptic response is normalized to a 2 min baseline. Inset: sample traces averaged from the baseline (thin lines) or from the last 10 min of the recording (thick lines). **B.** Similar to A, using slices pre-treated with the PTEN inhibitor bpV(HO)pic or control (untreated) slices. **C.** Average of AMPAR-mediated responses collected from the last 10 min of the recording (25-35 min in A, 40-50 min in B) and normalized to the baseline. Left and right columns (LTP, paired) correspond to the stimulation pathway in which postsynaptic depolarization (0 mV) was paired to presynaptic stimulation (3 Hz). Middle columns (control, unpaired) correspond to the pathway that was not stimulated during depolarization. “n” represents number of cells. **D.** mGluR-dependent LTD was induced by bath-application of 50 μM DHPG (agonist of type I mGluR receptors). Recordings were carried out in the presence of 100 μM AP5 (NMDAR antagonist) (see Methods). Synaptic responses were normalized to a 10 min baseline before DHPG application for uninfected neurons (white symbols) and for GFP-PTEN-C124S-expressing neurons (black symbols). Inset: sample traces averaged from the baseline (thin lines) or from the last 10 min of the recording (thick lines). **E.** Similar to D, using slices pre-treated with the PTEN inhibitor bpV(HO)pic or control (untreated) slices. **F.** Average of AMPAR-mediated responses collected from the last 10 min of the recording (50-60 min in D, 35-45 in E) and normalized to the baseline.

Figure 8. Involvement of the PDZ motif of PTEN in LTD. A. Sample traces of evoked AMPAR- and NMDAR-mediated synaptic responses recorded at -60 mV or +40 mV, respectively, from CA1 neurons expressing GFP-PTEN-C124S-ΔPDZ and neighboring control (uninfected) neurons. **B.** Average AMPAR-mediated current amplitude (peak of the synaptic response recorded at -60 mV) from pairs of uninfected and GFP-PTEN-C124S-ΔPDZ-expressing neurons. For B and C, "n" represents number of pairs of cells, and statistical significance was determined with the Wilcoxon test. **C.** Average NMDAR-mediated current amplitude (recorded at +40 mV and measured at a latency of 60 ms) from pairs of uninfected and GFP-PTEN-C124S-ΔPDZ-expressing neurons. **D.** LTD was induced in CA1 hippocampal neurons expressing GFP-PTEN-C124S-ΔPDZ (black symbols) or in control (uninfected) neurons (white symbols). Amplitude of the synaptic responses is normalized to a 10 min baseline. Insets: sample traces averaged from the baseline (thin lines) or from the last 10 min of the recording (thick lines). **E.** Average of AMPAR-mediated responses collected from the last 10 min of the recording and normalized to the baseline. Left columns (LTD, paired) correspond to the stimulation pathway in which postsynaptic depolarization (-40 mV) was paired to low-frequency stimulation (1 Hz). Right columns (control, unpaired) correspond to the pathway that was not stimulated during depolarization. "n" represents number of cells.

REFERENCES

Arendt, K.L., Royo, M., Fernandez-Monreal, M., Knafo, S., Petrok, C.N., Martens, J.R. and Esteban, J.A. (2010) PIP3 controls synaptic function by maintaining AMPA receptor clustering at the postsynaptic membrane. *Nat Neurosci*, **13**, 36-44.

Backman, S.A., Stambolic, V., Suzuki, A., Haight, J., Elia, A., Pretorius, J., Tsao, M.S., Shannon, P., Bolon, B., Ivy, G.O. and Mak, T.W. (2001) Deletion of Pten in mouse brain causes seizures, ataxia and defects in soma size resembling Lhermitte-Duclos disease. *Nat Genet*, **29**, 396-403.

Bhattacharyya, S., Biou, V., Xu, W., Schluter, O. and Malenka, R.C. (2009) A critical role for PSD-95/AKAP interactions in endocytosis of synaptic AMPA receptors. *Nat Neurosci*, **12**, 172-181.

Blanpied, T.A., Scott, D.B. and Ehlers, M.D. (2002) Dynamics and regulation of clathrin coats at specialized endocytic zones of dendrites and spines. *Neuron*, **36**, 435-449.

Bonifant, C.L., Kim, J.S. and Waldman, T. (2007) NHERFs, NEP, MAGUKs, and more: interactions that regulate PTEN. *J Cell Biochem*, **102**, 878-885.

Brunet, A., Datta, S.R. and Greenberg, M.E. (2001) Transcription-dependent and -independent control of neuronal survival by the PI3K-Akt signaling pathway. *Curr Opin Neurobiol*, **11**, 297-305.

Butler, M.G., Dasouki, M.J., Zhou, X.P., Talebizadeh, Z., Brown, M., Takahashi, T.N., Miles, J.H., Wang, C.H., Stratton, R., Pilarski, R. and Eng, C. (2005) Subset of individuals with autism spectrum disorders and extreme macrocephaly associated with germline PTEN tumour suppressor gene mutations. *J Med Genet*, **42**, 318-321.

Cammalleri, M., Lutjens, R., Berton, F., King, A.R., Simpson, C., Francesconi, W. and Sanna, P.P. (2003) Time-restricted role for dendritic activation of the mTOR-p70S6K pathway in the induction of late-phase long-term potentiation in the CA1. *Proc Natl Acad Sci U S A*, **100**, 14368-14373.

Carlin, R.K., Grab, D.J., Cohen, R.S. and Siekevitz, P. (1980) Isolation and characterization of postsynaptic densities from various brain regions: enrichment of different types of postsynaptic densities. *J Cell Biol*, **86**, 831-845.

Chadborn, N.H., Ahmed, A.I., Holt, M.R., Prinjha, R., Dunn, G.A., Jones, G.E. and Eickholt, B.J. (2006) PTEN couples Sema3A signalling to growth cone collapse. *J Cell Sci*, **119**, 951-957.

Chen, X., Garelick, M.G., Wang, H., Lil, V., Athos, J. and Storm, D.R. (2005) PI3 kinase signaling is required for retrieval and extinction of contextual memory. *Nat Neurosci*, **8**, 925-931.

Collingridge, G.L., Olsen, R.W., Peters, J. and Spedding, M. (2009) A nomenclature for ligand-gated ion channels. *Neuropharmacology*, **56**, 2-5.

Cross, D.A., Alessi, D.R., Cohen, P., Andjelkovich, M. and Hemmings, B.A. (1995) Inhibition of glycogen synthase kinase-3 by insulin mediated by protein kinase B. *Nature*, **378**, 785-789.

Ehrlich, I. and Malinow, R. (2004) Postsynaptic density 95 controls AMPA receptor incorporation during long-term potentiation and experience-driven synaptic plasticity. *J Neurosci*, **24**, 916-927.

El-Husseini, A.E., Schnell, E., Chetkovich, D.M., Nicoll, R.A. and Bredt, D.S. (2000) PSD-95 involvement in maturation of excitatory synapses. *Science*, **290**, 1364-1368.

Eng, C. (2003) PTEN: one gene, many syndromes. *Hum Mutat*, **22**, 183-198.

Fraser, M.M., Bayazitov, I.T., Zakharenko, S.S. and Baker, S.J. (2008) Phosphatase and tensin homolog, deleted on chromosome 10 deficiency in brain causes defects in synaptic structure, transmission and plasticity, and myelination abnormalities. *Neuroscience*, **151**, 476-488.

Futai, K., Kim, M.J., Hashikawa, T., Scheiffele, P., Sheng, M. and Hayashi, Y. (2007) Retrograde modulation of presynaptic release probability through signaling mediated by PSD-95-neuroligin. *Nat Neurosci*, **10**, 186-195.

Hooper, C., Markevich, V., Plattner, F., Killick, R., Schofield, E., Engel, T., Hernandez, F., Anderton, B., Rosenblum, K., Bliss, T., Cooke, S.F., Avila, J., Lucas, J.J., Giese, K.P., Stephenson, J. and Lovestone, S. (2007) Glycogen synthase kinase-3 inhibition is integral to long-term potentiation. *Eur J Neurosci*, **25**, 81-86.

Horne, E.A. and Dell'Acqua, M.L. (2007) Phospholipase C is required for changes in postsynaptic structure and function associated with NMDA receptor-dependent long-term depression. *J Neurosci*, **27**, 3523-3534.

Jaworski, J., Spangler, S., Seeburg, D.P., Hoogenraad, C.C. and Sheng, M. (2005) Control of dendritic arborization by the phosphoinositide-3'-kinase-Akt-mammalian target of rapamycin pathway. *J Neurosci*, **25**, 11300-11312.

Kwon, C.H., Luikart, B.W., Powell, C.M., Zhou, J., Matheny, S.A., Zhang, W., Li, Y., Baker, S.J. and Parada, L.F. (2006) Pten regulates neuronal arborization and social interaction in mice. *Neuron*, **50**, 377-388.

Kwon, C.H., Zhu, X., Zhang, J., Knoop, L.L., Tharp, R., Smeyne, R.J., Eberhart, C.G., Burger, P.C. and Baker, S.J. (2001) Pten regulates neuronal soma size: a mouse model of Lhermitte-Duclos disease. *Nat Genet*, **29**, 404-411.

Lee, H.K., Kameyama, K., Huganir, R.L. and Bear, M.F. (1998) NMDA induces long-term synaptic depression and dephosphorylation of the GluR1 subunit of AMPA receptors in hippocampus. *Neuron*, **21**, 1151-1162.

Li, J., Yen, C., Liaw, D., Podsypanina, K., Bose, S., Wang, S.I., Puc, J., Miliaresis, C., Rodgers, L., McCombie, R., Bigner, S.H., Giovanella, B.C., Ittmann, M., Tycko, B., Hibshoosh, H., Wigler, M.H. and Parsons, R. (1997) PTEN, a putative protein tyrosine phosphatase gene mutated in human brain, breast, and prostate cancer. *Science*, **275**, 1943-1947.

Luscher, C., Xia, H., Beattie, E.C., Carroll, R.C., von Zastrow, M., Malenka, R.C. and Nicoll, R.A. (1999) Role of AMPA receptor cycling in synaptic transmission and plasticity. *Neuron*, **24**, 649-658.

Maehama, T. and Dixon, J.E. (1998) The tumor suppressor, PTEN/MMAC1, dephosphorylates the lipid second messenger, phosphatidylinositol 3,4,5-trisphosphate. *J Biol Chem*, **273**, 13375-13378.

Maehama, T. and Dixon, J.E. (1999) PTEN: a tumour suppressor that functions as a phospholipid phosphatase. *Trends Cell Biol*, **9**, 125-128.

Myers, M.P., Pass, I., Batty, I.H., Van der Kaay, J., Stolarov, J.P., Hemmings, B.A., Wigler, M.H., Downes, C.P. and Tonks, N.K. (1998) The lipid phosphatase activity of PTEN is critical for its tumor supressor function. *Proc Natl Acad Sci U S A*, **95**, 13513-13518.

Nishimune, A., Isaac, J.T., Molnar, E., Noel, J., Nash, S.R., Tagaya, M., Collingridge, G.L., Nakanishi, S. and Henley, J.M. (1998) NSF binding to GluR2 regulates synaptic transmission. *Neuron*, **21**, 87-97.

Oliet, S.H., Malenka, R.C. and Nicoll, R.A. (1997) Two distinct forms of long-term depression coexist in CA1 hippocampal pyramidal cells. *Neuron*, **18**, 969-982.

Opazo, P., Watabe, A.M., Grant, S.G. and O'Dell, T.J. (2003) Phosphatidylinositol 3-kinase regulates the induction of long-term potentiation through extracellular signal-related kinase-independent mechanisms. *J Neurosci*, **23**, 3679-3688.

Palmer, M.J., Irving, A.J., Seabrook, G.R., Jane, D.E. and Collingridge, G.L. (1997) The group I mGlu receptor agonist DHPG induces a novel form of LTD in the CA1 region of the hippocampus. *Neuropharmacology*, **36**, 1517-1532.

Peineau, S., Taghibiglou, C., Bradley, C., Wong, T.P., Liu, L., Lu, J., Lo, E., Wu, D., Saule, E., Bouschet, T., Matthews, P., Isaac, J.T., Bortolotto, Z.A., Wang, Y.T. and Collingridge, G.L. (2007) LTP inhibits LTD in the hippocampus via regulation of GSK3beta. *Neuron*, **53**, 703-717.

Pendaries, C., Tronchere, H., Plantavid, M. and Payrastre, B. (2003) Phosphoinositide signaling disorders in human diseases. *FEBS Lett*, **546**, 25-31.

Perandones, C., Costanzo, R.V., Kowaljow, V., Pivetta, O.H., Carminatti, H. and Radrizzani, M. (2004) Correlation between synaptogenesis and the PTEN phosphatase expression in dendrites during postnatal brain development. *Brain Res Mol Brain Res*, **128**, 8-19.

Petralia, R.S., Wang, Y.X. and Wenthold, R.J. (2003) Internalization at glutamatergic synapses during development. *Eur J Neurosci*, **18**, 3207-3217.

Phend, K.D., Rustioni, A. and Weinberg, R.J. (1995) An osmium-free method of epon embedment that preserves both ultrastructure and antigenicity for post-embedding immunocytochemistry. *J Histochem Cytochem*, **43**, 283-292.

Qin, Y., Zhu, Y., Baumgart, J.P., Stornetta, R.L., Seidenman, K., Mack, V., van Aelst, L. and Zhu, J.J. (2005) State-dependent Ras signaling and AMPA receptor trafficking. *Genes Dev*, **19**, 2000-2015.

Racz, B., Blanpied, T.A., Ehlers, M.D. and Weinberg, R.J. (2004) Lateral organization of endocytic machinery in dendritic spines. *Nat Neurosci*, **7**, 917-918.

Raghavachari, S. and Lisman, J.E. (2004) Properties of quantal transmission at CA1 synapses. *J Neurophysiol*, **92**, 2456-2467.

Regalado, M.P., Terry-Lorenzo, R.T., Waites, C.L., Garner, C.C. and Malenka, R.C. (2006) Transsynaptic signaling by postsynaptic synapse-associated protein 97. *J Neurosci*, **26**, 2343-2357.

Sanna, P.P., Cammalleri, M., Berton, F., Simpson, C., Lutjens, R., Bloom, F.E. and Francesconi, W. (2002) Phosphatidylinositol 3-kinase is required for the expression but not for the induction or the maintenance of long-term potentiation in the hippocampal CA1 region. *J Neurosci*, **22**, 3359-3365.

Schmid, A.C., Byrne, R.D., Vilar, R. and Woscholski, R. (2004) Bisperoxovanadium compounds are potent PTEN inhibitors. *FEBS Lett*, **566**, 35-38.

Sheng, M. (2001) Molecular organization of the postsynaptic specialization. *Proc Natl Acad Sci U S A*, **98**, 7058-7061.

Song, I., Kamboj, S., Xia, J., Dong, H., Liao, D. and Huganir, R.L. (1998) Interaction of the N-ethylmaleimide-sensitive factor with AMPA receptors. *Neuron*, **21**, 393-400.

Stambolic, V., Suzuki, A., de la Pompa, J.L., Brothers, G.M., Mirtsos, C., Sasaki, T., Ruland, J., Penninger, J.M., Siderovski, D.P. and Mak, T.W. (1998) Negative regulation of PKB/Akt-dependent cell survival by the tumor suppressor PTEN. *Cell*, **95**, 29-39.

Steck, P.A., Pershouse, M.A., Jasser, S.A., Yung, W.K., Lin, H., Ligon, A.H., Langford, L.A., Baumgard, M.L., Hattier, T., Davis, T., Frye, C., Hu, R., Swedlund, B., Teng, D.H. and

Tavtigian, S.V. (1997) Identification of a candidate tumour suppressor gene, MMAC1, at chromosome 10q23.3 that is mutated in multiple advanced cancers. *Nat Genet*, **15**, 356-362.

Stiles, B., Groszer, M., Wang, S., Jiao, J. and Wu, H. (2004) PTENless means more. *Dev Biol*, **273**, 175-184.

Sturgill, J.F., Steiner, P., Czervionke, B.L. and Sabatini, B.L. (2009) Distinct domains within PSD-95 mediate synaptic incorporation, stabilization, and activity-dependent trafficking. *J Neurosci*, **29**, 12845-12854.

Tamguney, T. and Stokoe, D. (2007) New insights into PTEN. *J Cell Sci*, **120**, 4071-4079.

Tang, S.J., Reis, G., Kang, H., Gingras, A.C., Sonenberg, N. and Schuman, E.M. (2002) A rapamycin-sensitive signaling pathway contributes to long-term synaptic plasticity in the hippocampus. *Proc Natl Acad Sci U S A*, **99**, 467-472.

Valiente, M., Andres-Pons, A., Gomar, B., Torres, J., Gil, A., Tapparel, C., Antonarakis, S.E. and Pulido, R. (2005) Binding of PTEN to specific PDZ domains contributes to PTEN protein stability and phosphorylation by microtubule-associated serine/threonine kinases. *J Biol Chem*, **280**, 28936-28943.

Wang, Y., Cheng, A. and Mattson, M.P. (2006) The PTEN phosphatase is essential for long-term depression of hippocampal synapses. *Neuromolecular Med*, **8**, 329-336.

Wu, X., Hepner, K., Castelino-Prabhu, S., Do, D., Kaye, M.B., Yuan, X.J., Wood, J., Ross, C., Sawyers, C.L. and Whang, Y.E. (2000) Evidence for regulation of the PTEN tumor suppressor by a membrane-localized multi-PDZ domain containing scaffold protein MAGI-2. *Proc Natl Acad Sci U S A*, **97**, 4233-4238.

Xu, W., Schluter, O.M., Steiner, P., Czervionke, B.L., Sabatini, B. and Malenka, R.C. (2008) Molecular dissociation of the role of PSD-95 in regulating synaptic strength and LTD. *Neuron*, **57**, 248-262.

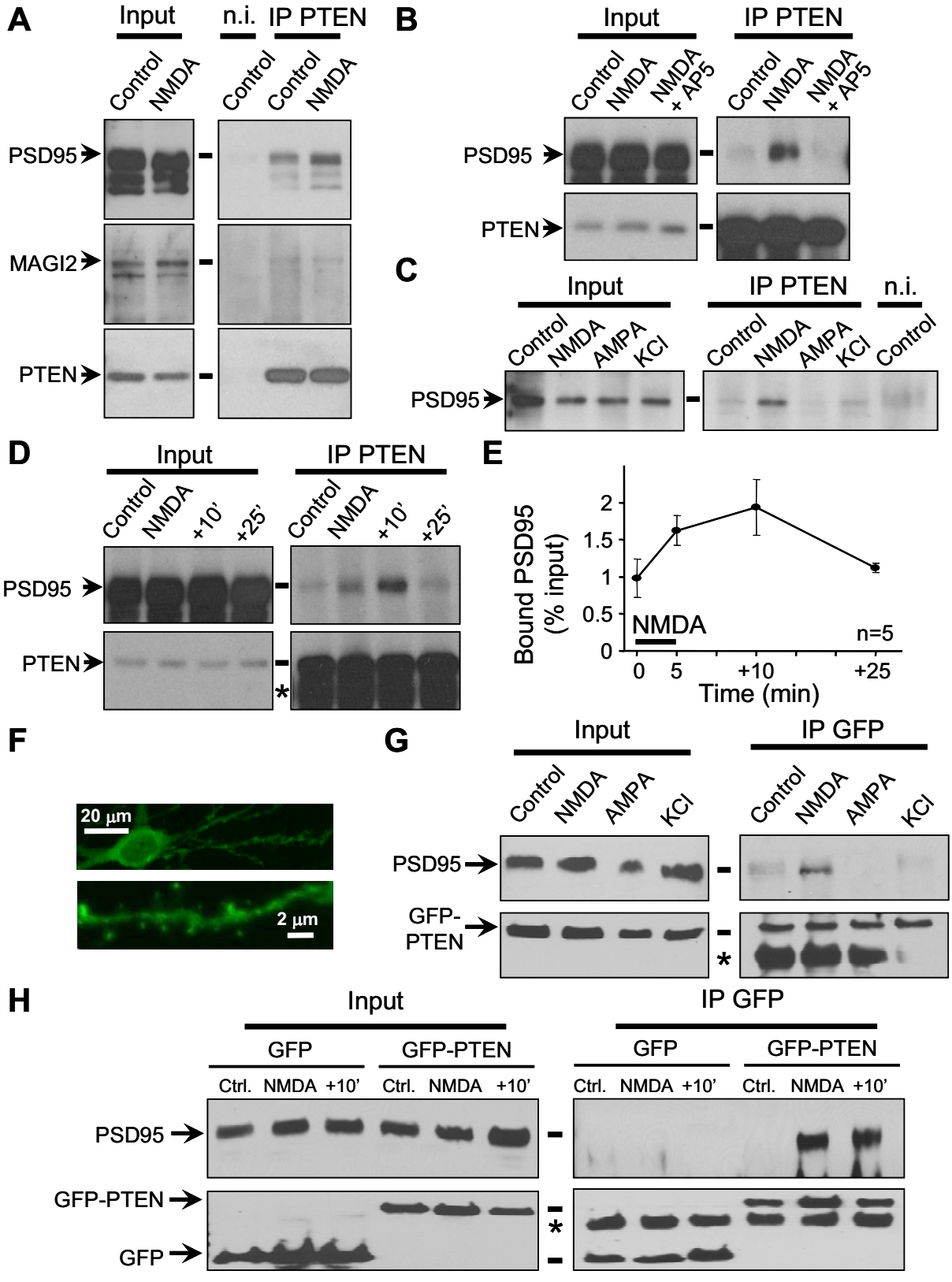
A
Input
n.i.
IP PTEN
Control
NMDA
Control
Control
NMDA
PSD95
MAGI2
PTEN
B
Input
IP PTEN
Control
NMDA
NMDA + AP5
Control
NMDA
NMDA + AP5
PSD95
PTEN
C
Input
IP PTEN
n.i.
Control
NMDA
AMPA
KCl
Control
NMDA
AMPA
KCl
Control
PSD95
D
Input
IP PTEN
Control
NMDA
+10'
+25'
Control
NMDA
+10'
+25'
PSD95
PTEN
*
E
Bound PSD95 (% input)
2
1.5
1
0.5
0
NMDA
n=5
0
5
+10
+25
Time (min)
F
20 µm
2 µm
G
Input
IP GFP
Control
NMDA
AMPA
KCl
Control
NMDA
AMPA
KCl
PSD95
GFP-PTEN
*
H
Input
IP GFP
GFP
GFP-PTEN
GFP
GFP-PTEN
Ctrl.
NMDA
+10'
Ctrl.
NMDA
+10'
Ctrl.
NMDA
+10'
Ctrl.
NMDA
+10'
PSD95
GFP-PTEN
GFP
*

Figure 1

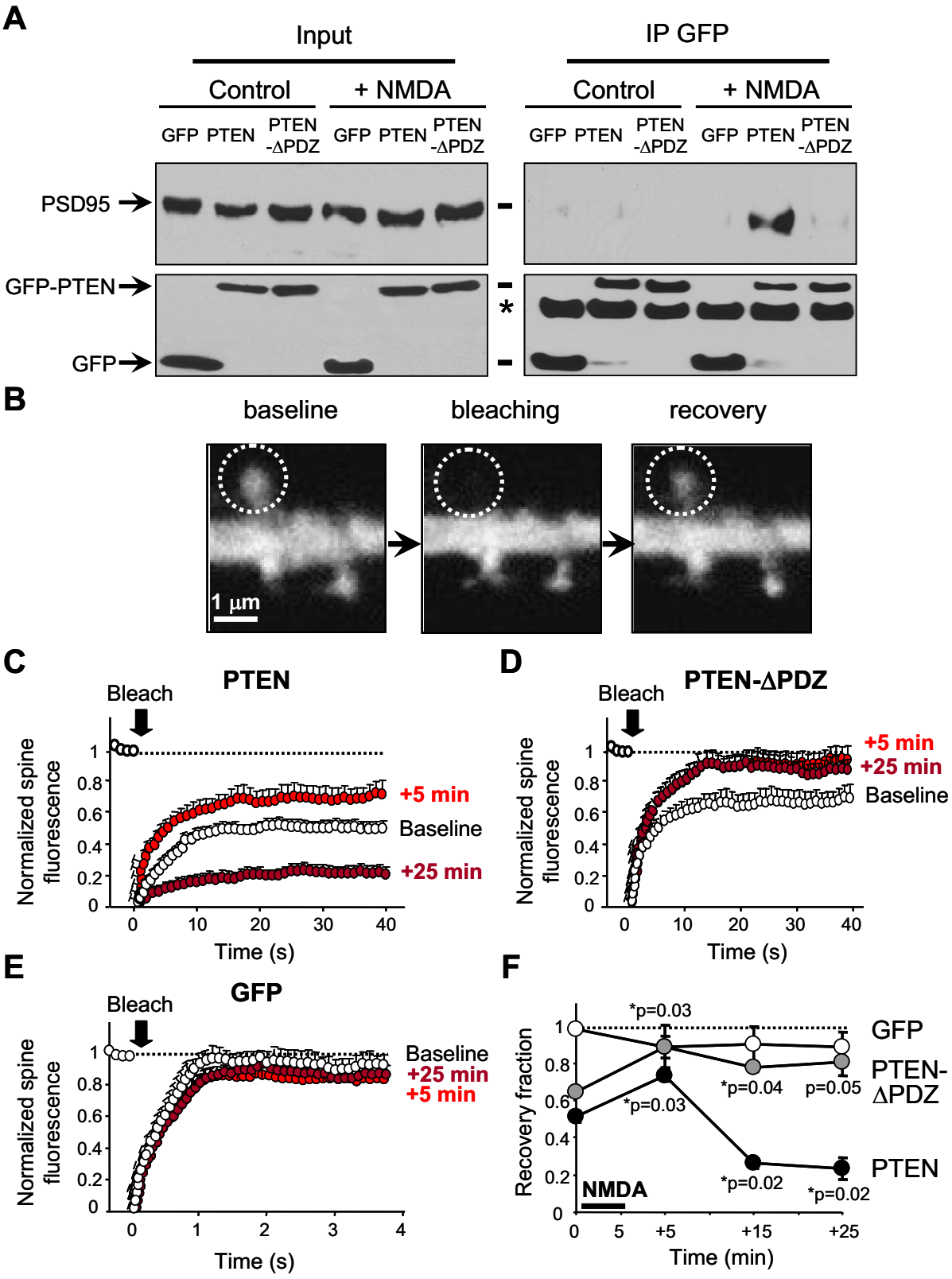
A
Input
IP GFP
Control
+ NMDA
Control
+ NMDA
GFP PTEN PTEN -ΔPDZ GFP PTEN PTEN -ΔPDZ
GFP PTEN PTEN -ΔPDZ GFP PTEN PTEN -ΔPDZ
PSD95
GFP-PTEN
GFP
*
B
baseline
bleaching
recovery
1 µm
C
PTEN
Bleach
Normalized spine fluorescence
+5 min
Baseline
+25 min
Time (s)
D
PTEN-ΔPDZ
Bleach
Normalized spine fluorescence
+5 min
+25 min
Baseline
Time (s)
E
GFP
Bleach
Normalized spine fluorescence
Baseline
+25 min
+5 min
Time (s)
F
Recovery fraction
*p=0.03
*p=0.04
p=0.05
*p=0.03
*p=0.02
*p=0.02
NMDA
GFP
PTEN-ΔPDZ
PTEN
Time (min)

Figure 2

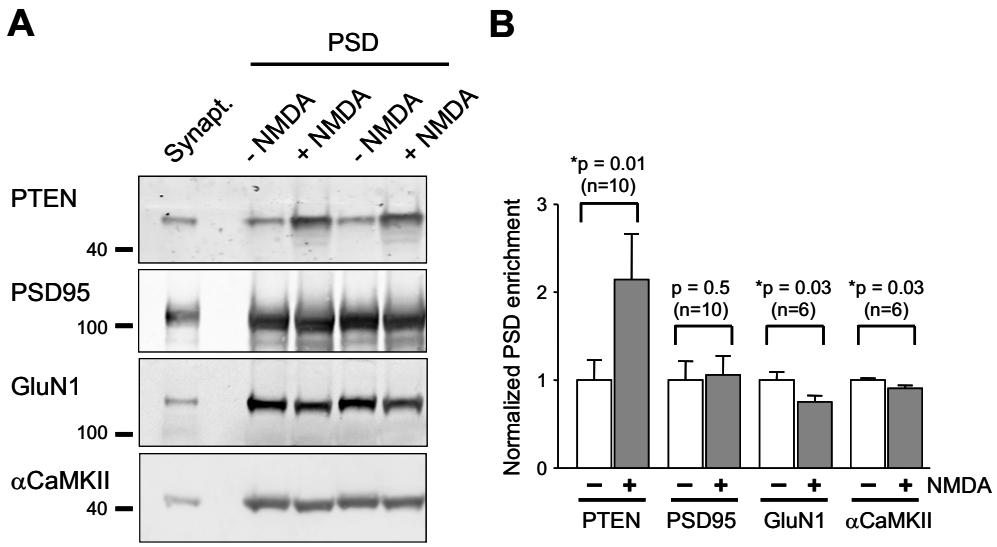
A
PSD
Synapt.
- NMDA
+ NMDA
- NMDA
+ NMDA
PTEN
40
PSD95
100
GluN1
100
αCaMKII
40
B
*p = 0.01
(n=10)
p = 0.5
(n=10)
*p = 0.03
(n=6)
*p = 0.03
(n=6)
Normalized PSD enrichment
3
2
1
0
− + − + − + − + NMDA
PTEN
PSD95
GluN1
αCaMKII

Figure 3

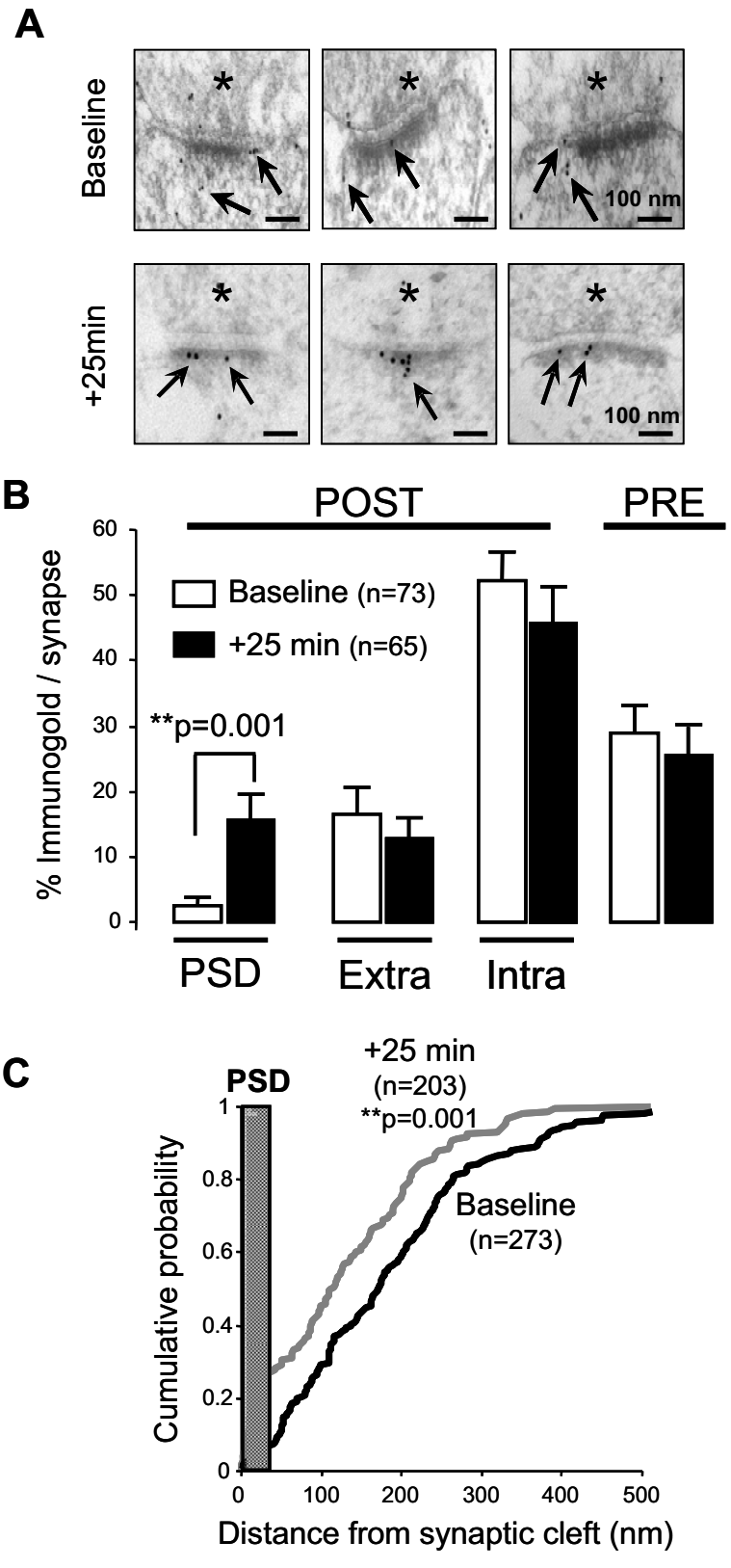
A
Baseline
+25min
100 nm
100 nm
B
POST
PRE
% Immunogold / synapse
Baseline (n=73)
+25 min (n=65)
**p=0.001
PSD
Extra
Intra
C
PSD
+25 min
(n=203)
**p=0.001
Baseline
(n=273)
Cumulative probability
Distance from synaptic cleft (nm)

Figure 4

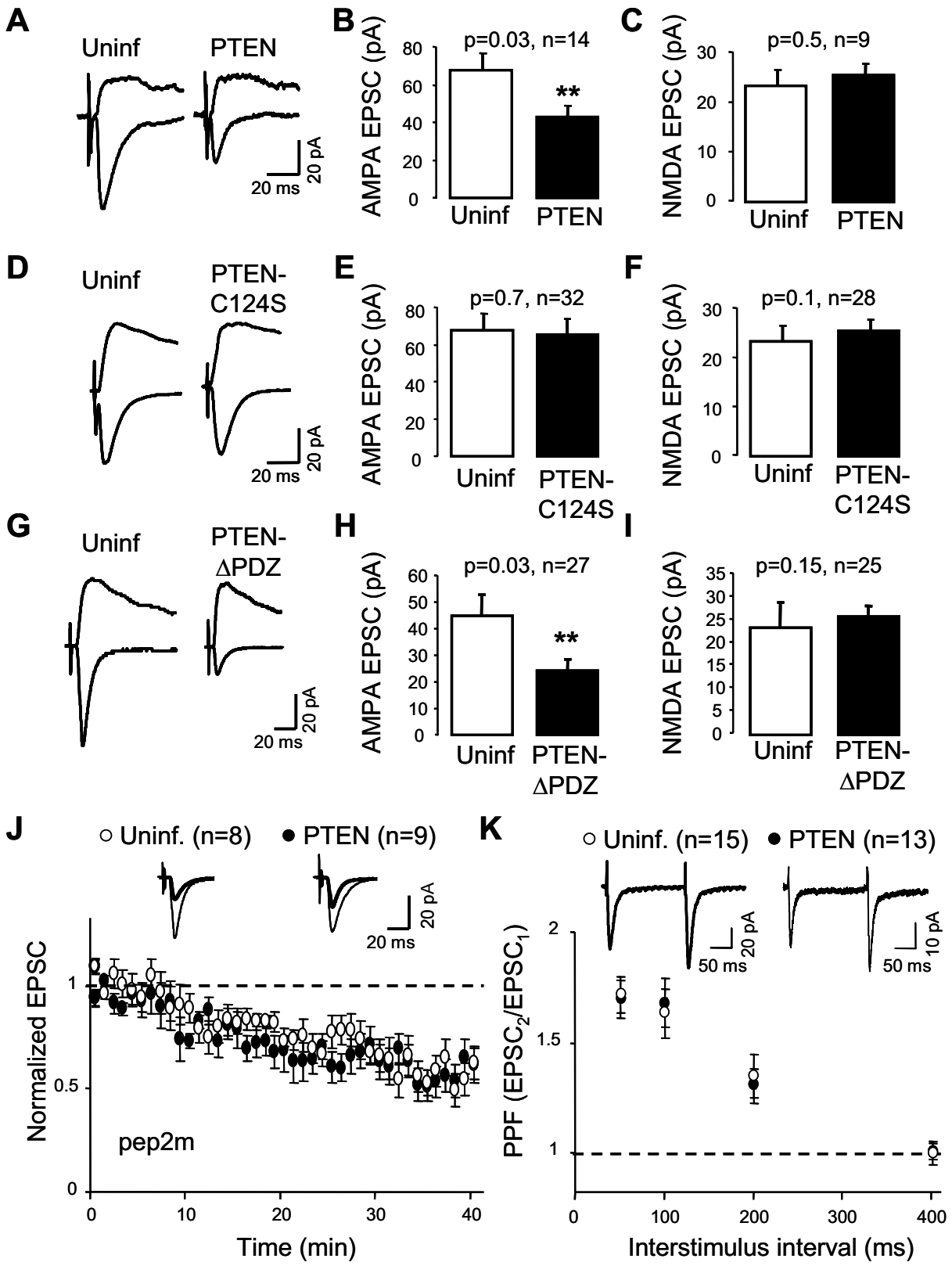
A
Uninf
PTEN
20 pA
20 ms
B
p=0.03, n=14
**
AMPA EPSC (pA)
Uninf
PTEN
C
p=0.5, n=9
NMDA EPSC (pA)
Uninf
PTEN
D
Uninf
PTEN-C124S
20 pA
20 ms
E
p=0.7, n=32
AMPA EPSC (pA)
Uninf
PTEN-C124S
F
p=0.1, n=28
NMDA EPSC (pA)
Uninf
PTEN-C124S
G
Uninf
PTEN-ΔPDZ
20 pA
20 ms
H
p=0.03, n=27
**
AMPA EPSC (pA)
Uninf
PTEN-ΔPDZ
I
p=0.15, n=25
NMDA EPSC (pA)
Uninf
PTEN-ΔPDZ
J
○ Uninf. (n=8)
● PTEN (n=9)
20 pA
20 ms
Normalized EPSC
pep2m
Time (min)
K
○ Uninf. (n=15)
● PTEN (n=13)
20 pA
50 ms
10 pA
50 ms
PPF (EPSC2/EPSC1)
Interstimulus interval (ms)

Figure 5

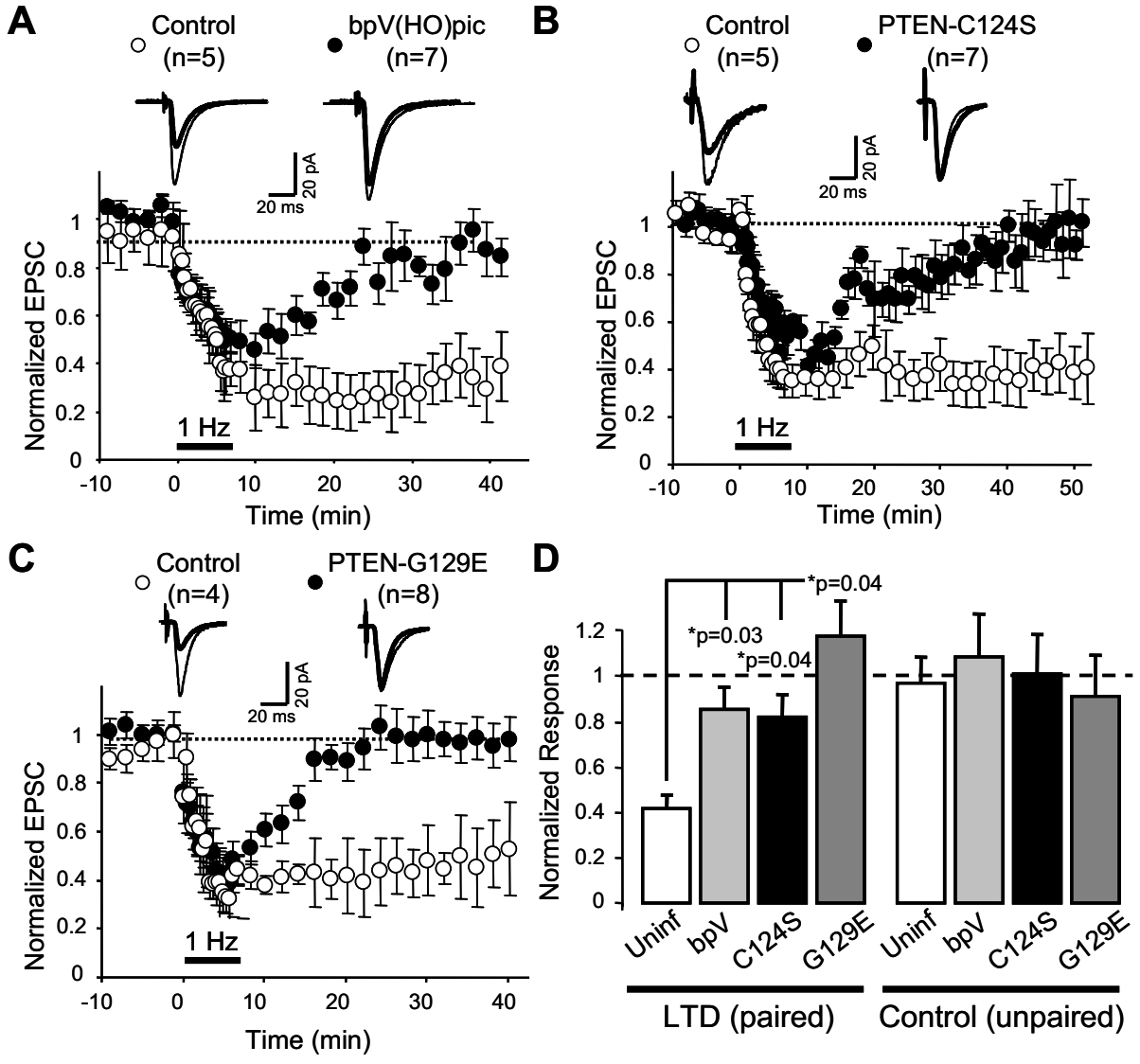
A
Control
(n=5)
bpV(HO)pic
(n=7)
20 pA
20 ms
Normalized EPSC
1 Hz
Time (min)
B
Control
(n=5)
PTEN-C124S
(n=7)
20 pA
20 ms
Normalized EPSC
1 Hz
Time (min)
C
Control
(n=4)
PTEN-G129E
(n=8)
20 pA
20 ms
Normalized EPSC
1 Hz
Time (min)
D
*p=0.04
*p=0.03
*p=0.04
Normalized Response
Uninf
bpV
C124S
G129E
Uninf
bpV
C124S
G129E
LTD (paired)
Control (unpaired)

Figure 6

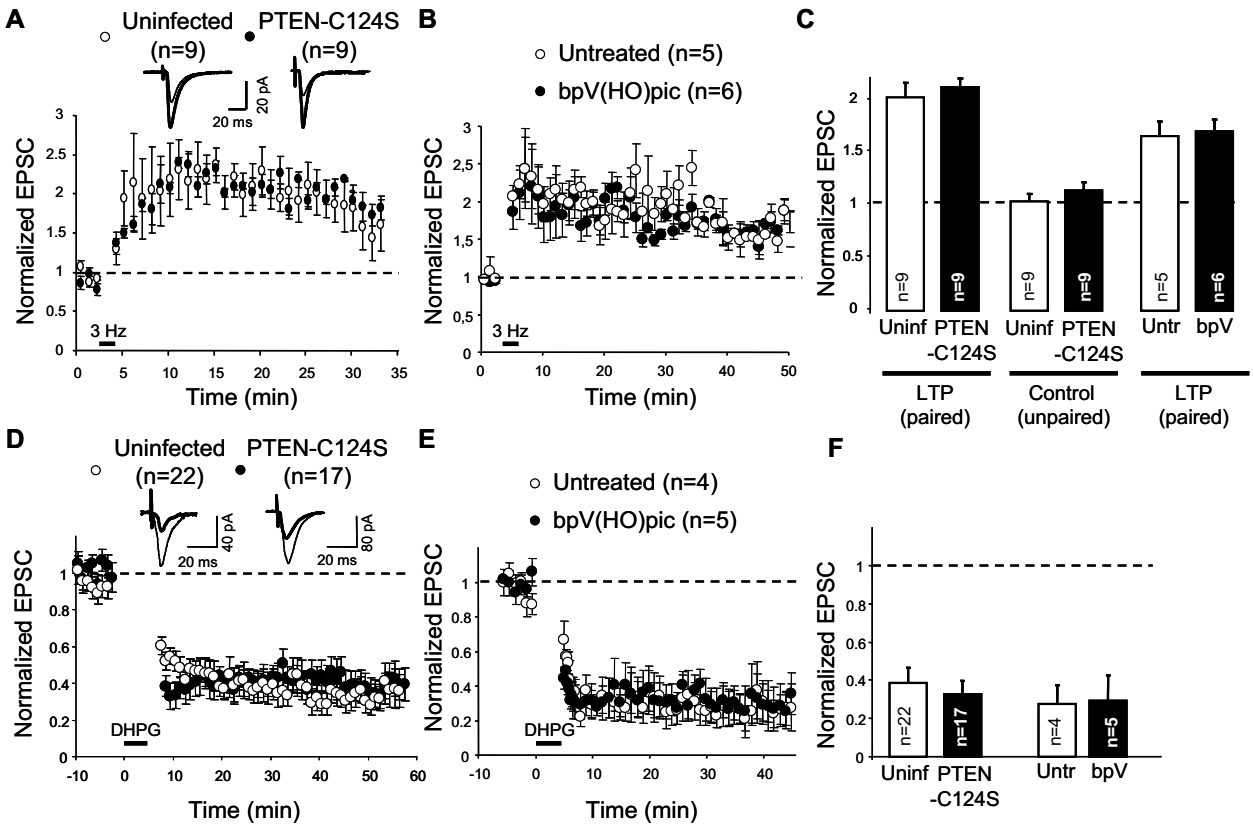
A
Uninfected (n=9)
PTEN-C124S (n=9)
20 pA
20 ms
Normalized EPSC
3 Hz
Time (min)
B
Untreated (n=5)
bpV(HO)pic (n=6)
Normalized EPSC
3 Hz
Time (min)
C
Normalized EPSC
n=9
n=9
n=9
n=9
n=5
n=6
Uninf
PTEN -C124S
Uninf
PTEN -C124S
Untr
bpV
LTP (paired)
Control (unpaired)
LTP (paired)
D
Uninfected (n=22)
PTEN-C124S (n=17)
40 pA
80 pA
20 ms
20 ms
Normalized EPSC
DHPG
Time (min)
E
Untreated (n=4)
bpV(HO)pic (n=5)
Normalized EPSC
DHPG
Time (min)
F
Normalized EPSC
n=22
n=17
n=4
n=5
Uninf
PTEN -C124S
Untr
bpV

Figure 7

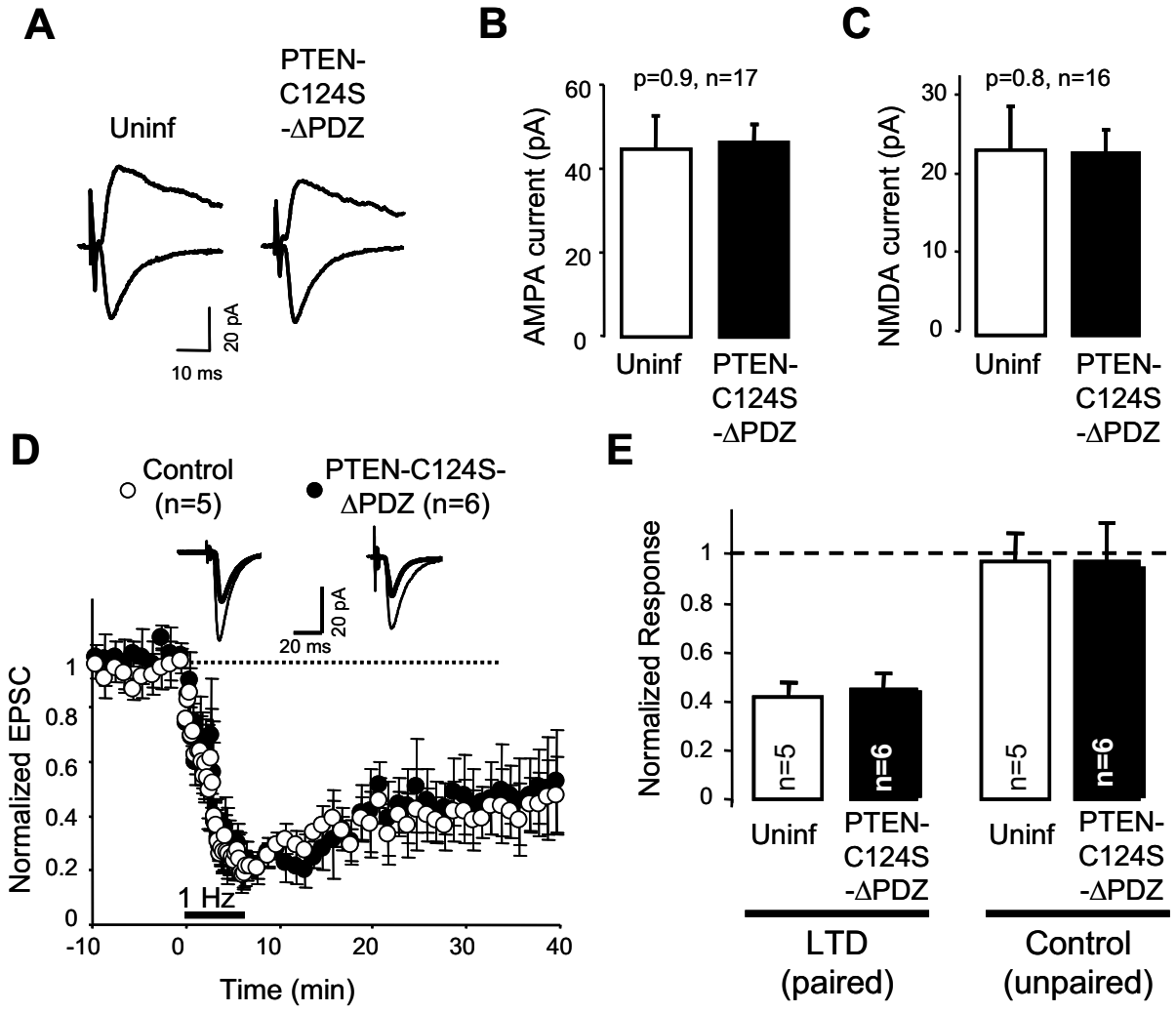
A
Uninf
PTEN-
C124S
-ΔPDZ
20 pA
10 ms
B
p=0.9, n=17
AMPA current (pA)
60
40
20
0
Uninf
PTEN-
C124S
-ΔPDZ
C
p=0.8, n=16
NMDA current (pA)
30
20
10
0
Uninf
PTEN-
C124S
-ΔPDZ
D
Control
(n=5)
PTEN-C124S-
ΔPDZ (n=6)
20 pA
20 ms
Normalized EPSC
1
0.8
0.6
0.4
0.2
0
1 Hz
-10
0
10
20
30
40
Time (min)
E
Normalized Response
1
0.8
0.6
0.4
0.2
0
n=5
n=6
n=5
n=6
Uninf
PTEN-
C124S
-ΔPDZ
Uninf
PTEN-
C124S
-ΔPDZ
LTD
(paired)
Control
(unpaired)

Figure 8

SUPPLEMENTARY METHODS

Construction of recombinant proteins and expression

The different GFP-tagged versions of PTEN were made by in-frame ligation of the EGFP coding sequence (Clontech) with the amino terminus of rat PTEN. The truncated form of PTEN (PTEN-ΔPDZ), lacking the C-terminal residues Ile^{400}-Thr^{401}-Lys^{402}-Val^{403}, the point mutants C124S and G129E, and the double mutant C124S-ΔPDZ were made by site-directed PCR mutagenesis. The catalytically inactive PTEN mutants (C124S and G129E) have been characterized previously (Myers et al., *Proc Natl Acad Sci USA*, **95**, 13513-13518, 1998). All constructs were prepared in pSinRep5 for expression using Sindbis virus. Recombinant proteins were expressed in hippocampal CA1 pyramidal neurons from organotypic slice cultures. Slices were prepared from postnatal day 5-7 rats and cultured from 5 to 10 days. Expression of the recombinant proteins was for 15 to 20 hours. All biosafety procedures and animal care protocols were approved by the University of Michigan Committee on Use and Care of Animals and the bioethics committee of the Consejo Superior de Investigaciones Científicas (CSIC).

Antibodies

Antibodies used in this study were: PTEN (Neomarkers -mouse, Cell Signalling -rabbit); PSD-95 (Neuromab -mouse, Abcam -rabbit); MAGI-2 and αCaMKII (Sigma); Akt, phospho-Akt (Ser473) and phospho-Tyrosine (Cell Signalling); GluA1, phospho-GluA1 (Ser831 and Ser845), GluA2, phospho-GluA2 (Ser880) and GluN1 (Millipore); GFP (Roche).

Synaptosomal/PSD fractionations and *in vitro* activation of NMDA receptors

Biochemical isolation of synaptosomes and PSD fractions were carried out essentially as previously described (Carlin et al., *J Cell Biol*, **86**, 831-845, 1980). Briefly, hippocampi from 3-4 week rats were homogenize in a Dounce glass homogenizer with buffer A (0.32 M sucrose, 1 mM $MgCl_2$, 0.5 mM $CaCl_2$, 10 mM HEPES, 1 mM EGTA, 1 mM dithiothreitol and a cocktail of protease inhibitors from Roche –"Complete Mini EDTA-free"). This homogenate was spun down at 1400g for 10 min at 4°C. The supernatant was kept and the pellet was resuspended in buffer A and spun again at 710g for 10 min at 4°C. Both supernatants were mixed and spun down at 11,600g for 12 min at 4°C. The pellet (crude synaptosomal fraction) was resupended in buffer B (10 mM HEPES, 1 mM dithiothreitol, protease inhibitor cocktail) plus 0.32 M sucrose, and overlaid on a discontinuous density gradient containing two layers of buffer B plus 1.0 M and 1.4 M sucrose. After centrifugation at 82,500g for 1 hour at 4°C, the interphase between 1.0 M and 1.4 M was collected (synaptosomal fraction).

The NMDA receptor activation was induced on the purified synaptosomes by adding 1.2 mM $MgCl_2$, 2.5 mM $CaCl_2$, 20 μM of NMDA and 10 μM glycine, and incubating for 5 min at room temperature. The reaction was stopped by addition of 100 μM DL-2-Amino-5-phosphonovaleric acid (AP-5) and 1 mM EDTA. After 10 min incubation at room temperature, the fractionation was continued by adding 0.5% Triton X-100 and stirring for 15 min at 4 °C. Then, samples were spun down at 165,000g for 2h at 4°C to obtain the Triton insoluble pellet (PSD fraction). This pellet was resuspended in 5% SDS and analyzed by 7% PAGE-SDS and western blot.

Electrophysiology methods

Solutions: The recording chamber was perfused with ACSF: 119 mM NaCl, 2.5 mM KCl, 4 mM $CaCl_2$, 4 mM $MgCl_2$, 26 mM NaHCO3, 1 mM NaH_2PO_4, 11 mM glucose, 0.1 mM picrotoxin, and 4 μM 2-chloroadenosine (pH 7.4), gassed with 5% CO_2 / 95% O_2. Patch recording pipettes (3-6 MΩ) were filled with 115 mM cesium methanesulfonate, 20 mM CsCl, 10 mM HEPES, 2.5 mM $MgCl_2$, 4 mM Na_2ATP, 0.4 mM Na_3GTP, 10 mM sodium phosphocreatine, 0.6 mM EGTA (pH 7.25). In experiments with intracellular perfusion of peptide pep2m/G10 (Tocris; 0.5 mM final concentration), the patch recording pipette solution was supplemented with protease inhibitors leupeptin and pepstatin (100 mM each).

Synaptic plasticity methods: NMDAR-dependent LTD was induced by pairing low-frequency presynaptic stimulation (500 pulses at 1 Hz) with moderate postsynaptic depolarization (–40 mV). LTP was induced by pairing 3 Hz presynaptic stimulation (300 pulses) with postsynaptic depolarization at 0 mV. In LTD and LTP experiments, one pathway did not receive stimulation during depolarization, and therefore was used as a control pathway. mGluR-dependent LTD was induced by bath application of 50 μM (RS)-3,5-dihydroxyphenylglycine (DHPG) for 5 min. Cells were held under current clamp without synaptic stimulation during DHPG application and 5 minutes afterwards (Huber et al., *J Neurophysiol*, **86**, 321-325, 2001). These recordings were carried out in the presence of 100 μM (2R)-amino-5-phosphonovaleric acid (APV), to prevent any contribution to synaptic plasticity from NMDARs. When blocking PTEN activity, slices were incubated with 15 nM bpV(HO)pic for 15-20 hours before LTD or LTP induction. bpV(HO)pic was also present during the recordings.

SUPPLEMENTARY FIGURE LEGENDS

Supplementary Figure 1. Specificity of the NMDA receptor-dependent association between PTEN and PSD-95. **A**. Total protein extracts from hippocampal slices were immunoprecipitated with anti-PSD95 antibody. Some slices were treated with 20 μM NMDA for 5 min before the immunoprecipitation and transferred to regular ACSF for 15, 25 or 60 min (+15', +25' or +60', as indicated). For the two right-most lanes, slices were preincubated with the NMDA receptor antagonist AP5 (100 μM) before and during the NMDA treatment (+AP5). Input lanes (left) contain 10% of the input from the baseline condition (without NMDA treatment). Coimmunoprecipitations were analyzed by western blot using PTEN and GluN1 antibodies, as indicated. **B**. Similar to A, with slices pretreated for 5 min with 20 μM NMDA, and transferred to regular ACSF for 15 min (+15') or 25 min (+25') after the NMDA treatment. Differences in protein migration between panels A and B can be explained by the different types of gels used (4–12% gradient Bis-Tris gels from Invitrogen –A–, *versus* custom-made gradient polyacrylamide gels –B–). Appropriate protein markers were used to estimate the molecular weight in each case. Star (*) indicates the position of the IgG used for immunoprecipitation in both experiments.

Supplementary Figure 2. Expression of recombinant PTEN variants and effect on the PI3K pathway. A. Western blot analysis of the phosphorylation of Akt at Ser473 from hippocampal slices expressing GFP, wild-type GFP-PTEN or the catalytically dead mutant GFP-PTEN-C124S. **B.** Quantification of Akt phosphorylation from three experiments as the one shown in A. Akt phosphorylation relative to total Akt levels was normalized to the values obtained from

GFP-expressing slices. **C.** Western blot analysis of the expression of recombinant GFP-PTEN, the point mutants C124S and G129E, the truncated mutant ΔPDZ and the double mutant C124S-ΔPDZ. Recombinant (GFP-fused) and endogenous PTEN were detected with an anti-PTEN antibody.

Supplementary Figure 3. FRAP fluorescence recovery rates and PTEN distribution between spines and dendrites are not altered by NMDA receptor activation. A. Fluorescence recovery time constants were estimated by exponential fits to the time courses shown in Fig. 2C-E. Values are plotted for untreated slices (0 min) or at different times after the 5 min NMDA treatment (black bar). Average values ± s.e.m. are plotted for GFP-PTEN (black symbols), GFP-PTEN-ΔPDZ (grey symbols) and GFP (white symbols). There was no significant change in FRAP time constant before and after NMDA treatment. **B.** Net GFP signal from GFP-PTEN (black symbols), GFP-PTEN-ΔPDZ (grey symbols) and GFP (white symbols) was quantified at spines and the adjacent dendritic shafts at different times, as described in A. The partition of these proteins between spines and dendrites (spine/dendrite ratio) was not significantly altered along the course of the experiment.

Supplementary Figure 4. Effects of recombinant PTEN expression on passive membrane properties of CA1 hippocampal neurons. A-C. The expression of GFP-PTEN, the point mutant C124S, the truncated mutant ΔPDZ and the double mutant C124S-ΔPDZ in CA1 hippocampal neurons did not alter input resistance (A), holding current (B) or whole-cell capacitance (C) when compared with uninfected control neurons. “n” represents number of cells.

Supplementary Figure 5. Overexpression of wild-type or dominant negative (C124S) PTEN does not alter GluA1 or GluA2 phosphorylation. A. Western blot analysis of GluA1, GluA2 and their phosphorylated forms (p-S880 for GluA2, p-S831 and p-S845 for GluA1) from hippocampal slices expressing GFP, GFP-PTEN or GFP-PTEN-C124S. **B.** Quantification of total and phosphorylated GluA1 and GluA2 from three experiments as the one shown in A. Values are normalized to GFP-infected slices (dashed line).

Supplementary Figure 6. Characterization of bpV(HO)pic as a specific PTEN inhibitor. A. Hippocampal slices expressing GFP-PTEN or uninfected were treated with different concentrations of bisperoxo(5-hydroxypyridine-2-carboxyl)oxovanadate (bpV(HO)pic) (Schmid et al., FEBS Lett. 566, 35-38, 2004), as indicated. After 16 hours, total protein extracts were prepared and analyzed by western blot with antibodies for phospho-Akt (Ser473), total Akt and phospho-tyrosine. Note the decrease in phospho-Akt in GFP-PTEN-expressing neurons, which is recovered with low (15 nM) concentrations of bpV(HO)pic. Phospho-tyrosine signal is only apparent at much higher (500 nM) concentrations. **B.** Quantification of phospho-Akt and phospho-tyrosine signal from three experiments as the one shown in A. The decrease in P-Akt signal in GFP-PTEN overexpressing slices is indicated with a star (*). P-Akt signal is recovered with 15 nM bpV(HO)pic, without affecting phospho-Tyr signal, indicating that low nanomolar concentrations of this compound selectively inhibit PTEN over phospho-Tyr phosphatases. These results essentially replicate previously published ones (Schmid et al., FEBS Lett. 566, 35-38, 2004).

Supplementary Figure 7. PTEN activity during LTD induction is necessary for LTD expression. LTD was induced in CA1 hippocampal neurons by pairing presynaptic stimulation (1 Hz, 500 pulses) with moderate postsynaptic depolarization (-40 mV) (black bar below graph). On some slices, the PTEN inhibitor bpV(HO)pic was applied 5 min before LTD induction and was washed out 5 min after the induction (black bar above graph). Treated slices are represented with white symbols, and untreated controls with black symbols. Amplitude of the synaptic response is normalized to a 5 min baseline. "n" represents number of cells. Statistical significance was calculated according to the Mann-Whitney test.

Supplementary Figure 8. PTEN overexpression does not affect LTD. A. LTD was induced in CA1 hippocampal neurons overexpressing wild-type PTEN (black symbols) or control, uninfected neurons (white symbols). Amplitude of the synaptic responses is normalized to a 10 min baseline. Insets: sample traces averaged from the baseline (thin lines) or from the last 10 min of the recording (thick lines). **B.** Average of AMPAR-mediated responses collected from the last 10 min of the recording and normalized to the baseline. Left columns (Paired, LTD) correspond to the stimulation pathway in which postsynaptic depolarization (-40 mV) was paired to low-frequency stimulation (1 Hz). Right columns (Control, unpaired) correspond to the pathway that was not stimulated during depolarization. "n" represents number of cells.

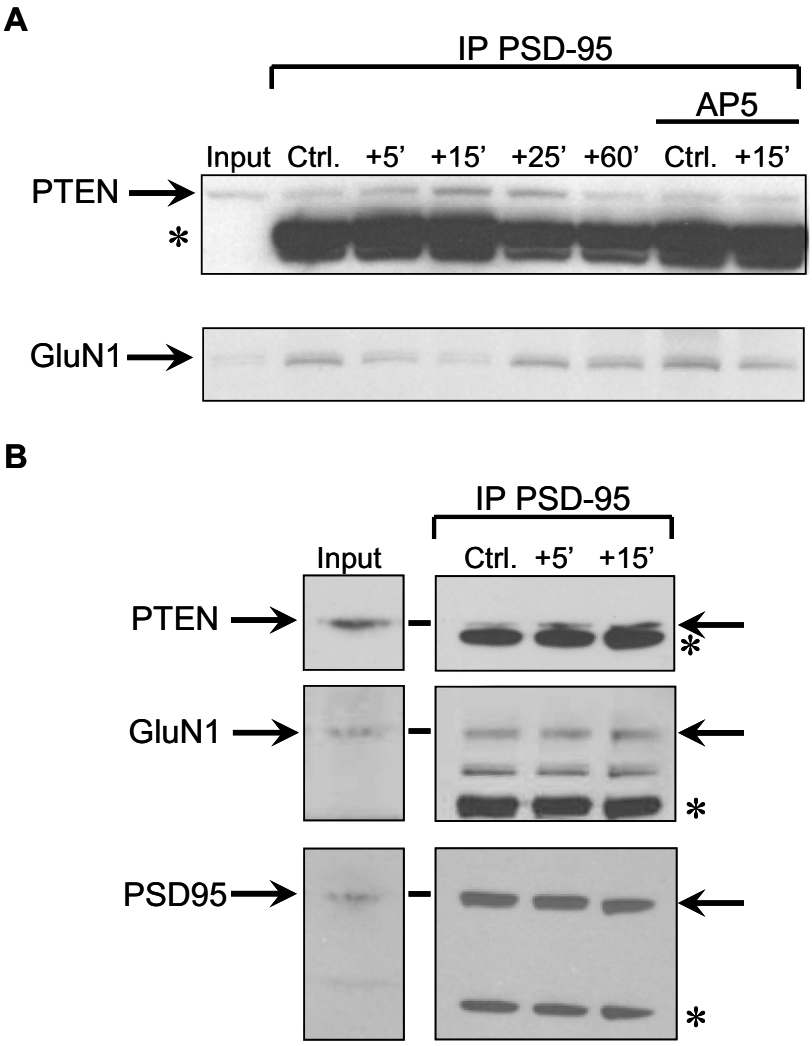

Supplementary Figure 1

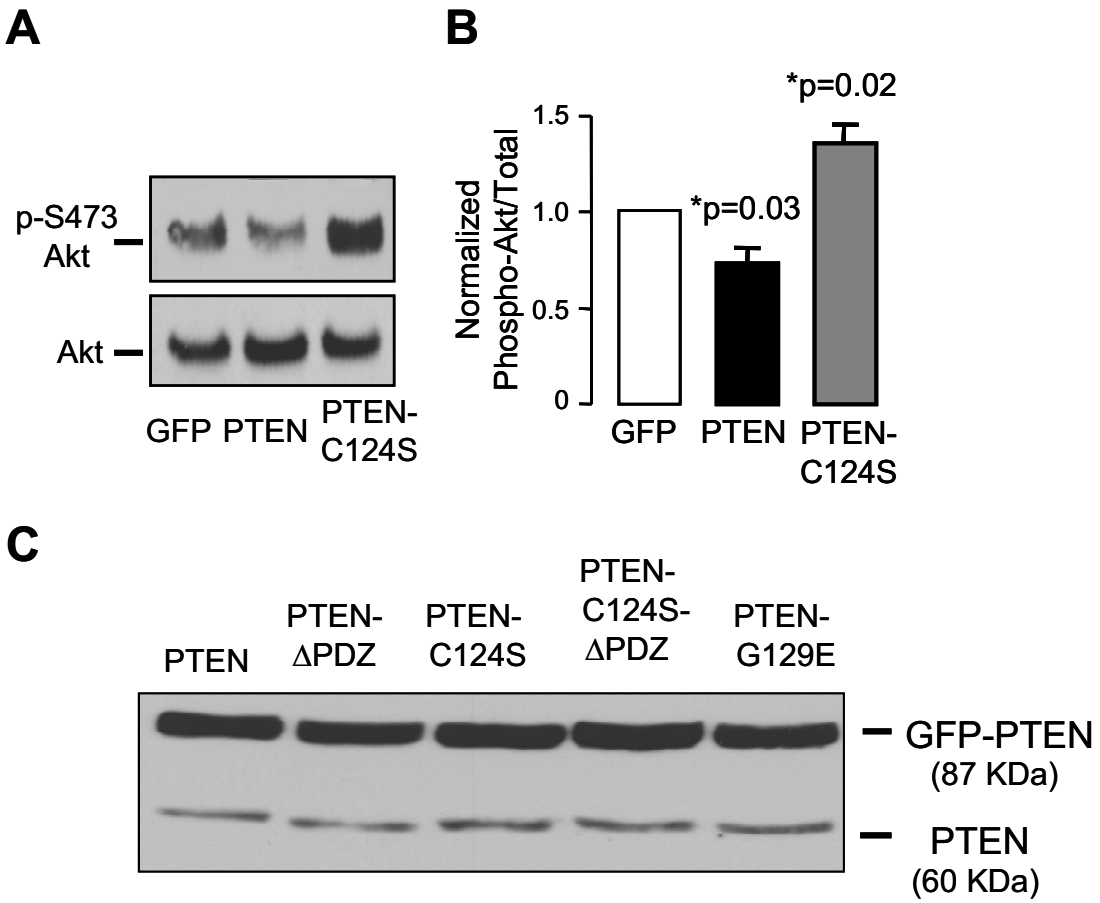

Supplementary Figure 2

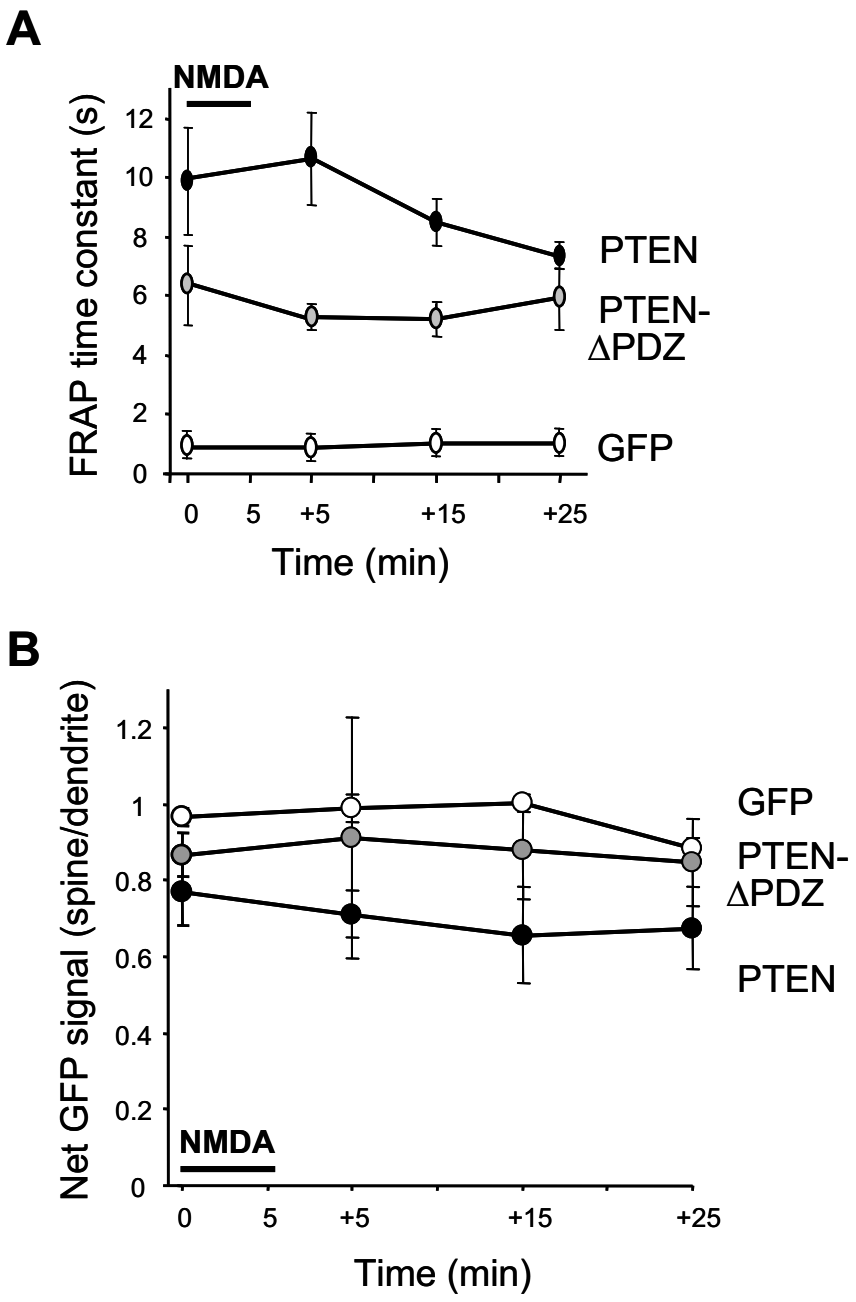

Supplementary Figure 3

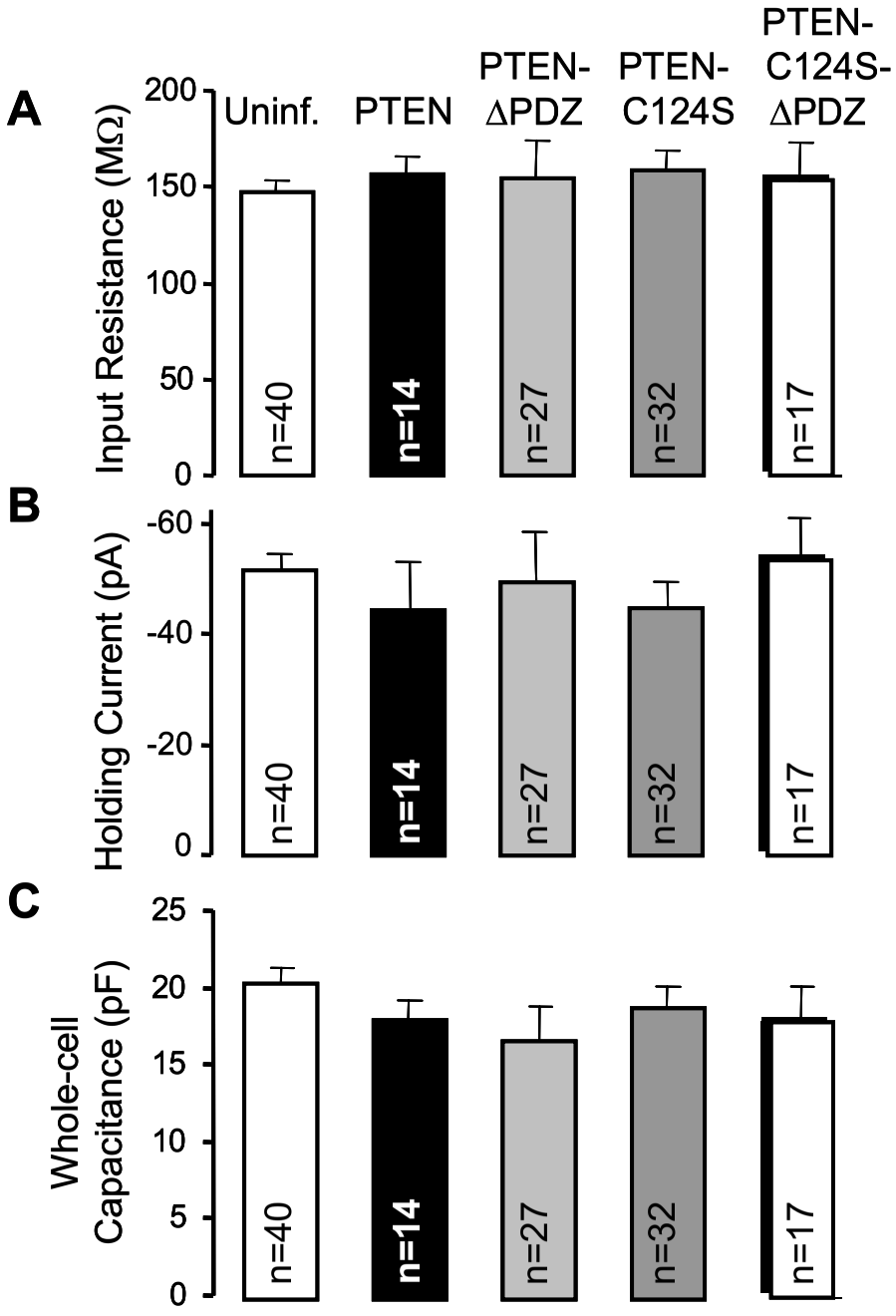

Supplementary Figure 4

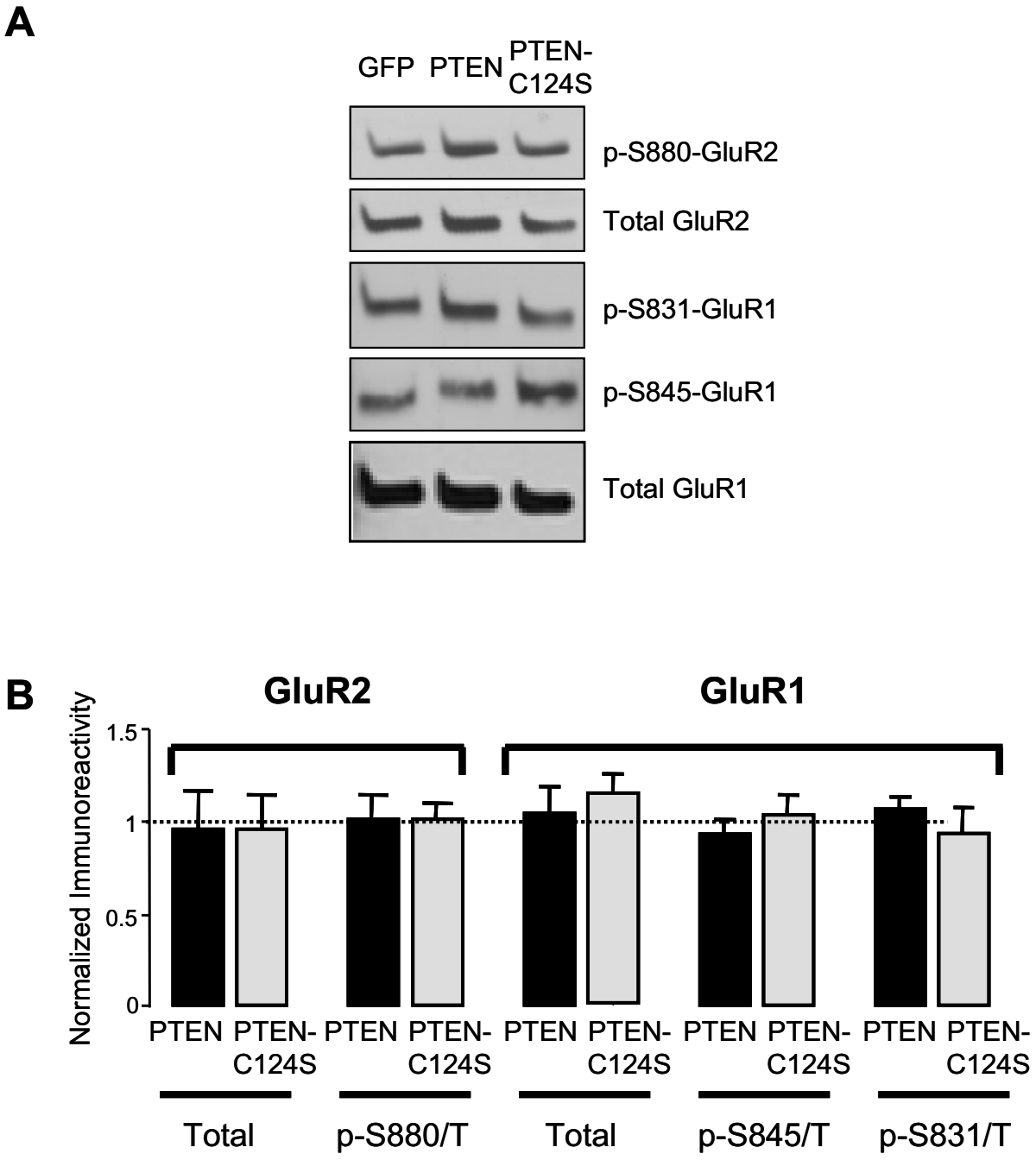

Supplementary Figure 5

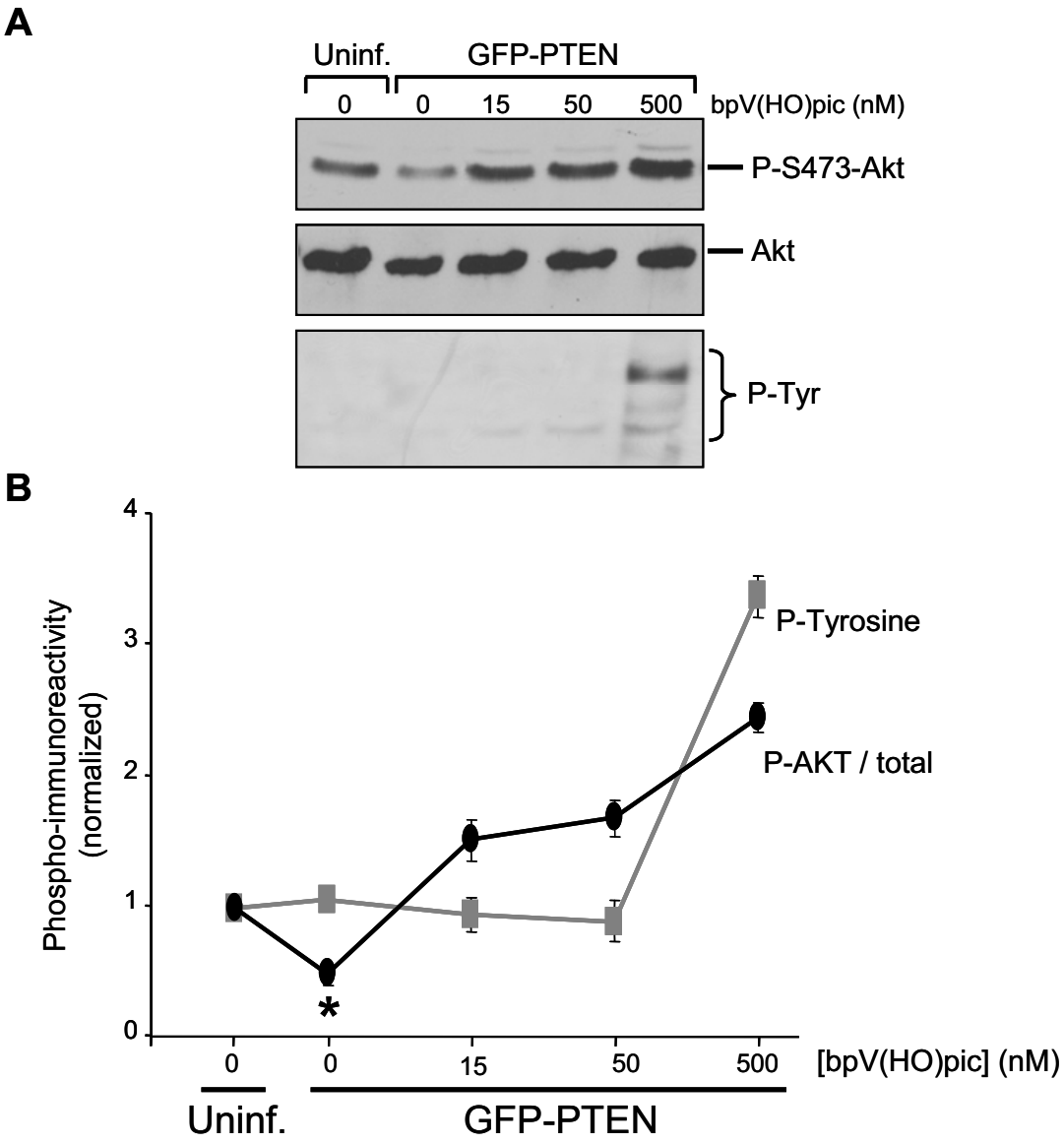

Supplementary Figure 6

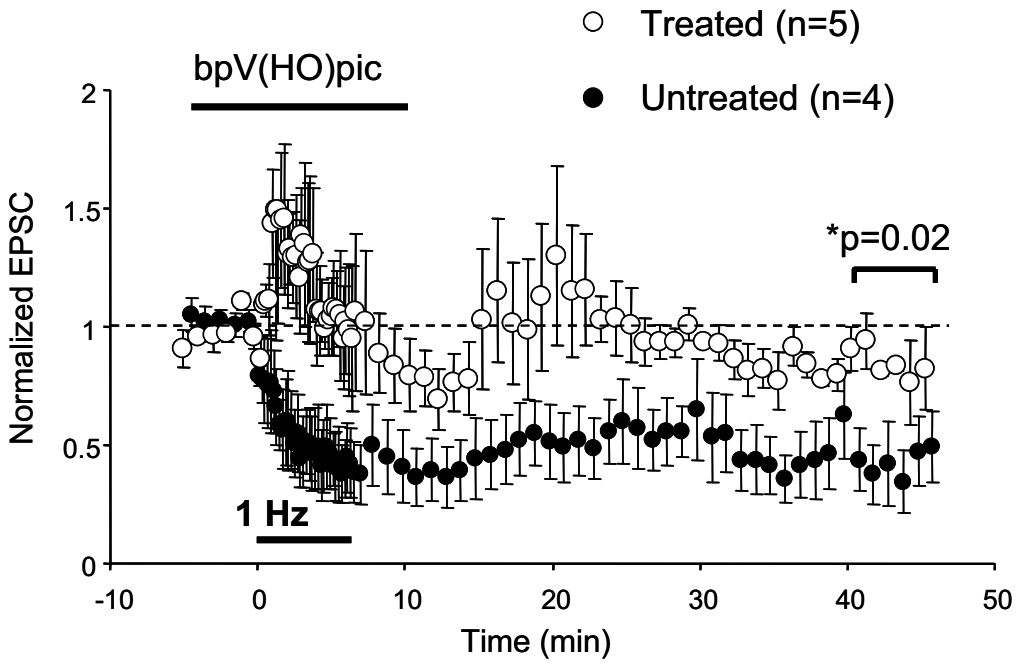

Supplementary Figure 7

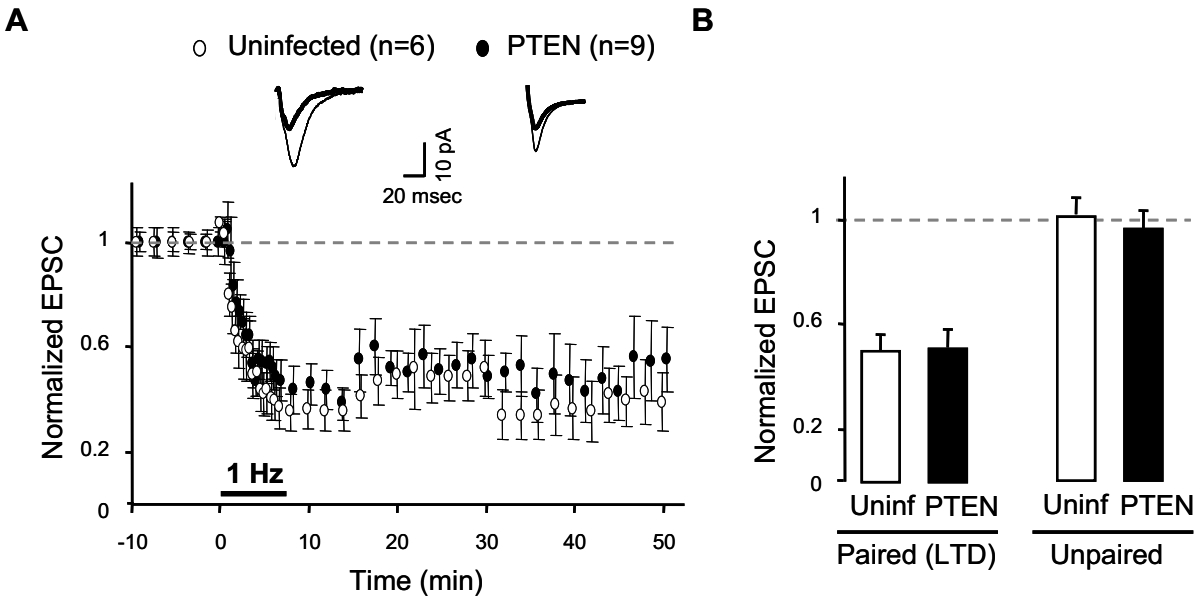

Supplementary Figure 8